# AMPLITUDE METHOD TO DETECT DEBONDING FOR STACK BOND ADHESIVE

by

XIAOBAO HUANG

A dissertation submitted in partial fulfillment of the
requirements for the degree of

DOCTOR OF PHILOSOPHY IN MECHANICAL ENGINEERING

2024

Oakland University
Rochester, Michigan

*To my mother and father:*
*Thank you for giving me the courage to do what I think it's right.*

ACKNOWLEDGMENTS

I cannot express enough thanks to my committee for their continued support and encouragement: Dr. Gary Barber, my committee chair; Dr. Rany Gu; Dr. Michael Latcha; Dr. Xia Wang; Dr. Hongwei Qu and Dr. Jun Zhou. I offer my sincere appreciation for the learning opportunities provided by my committee.

My completion of this study could not have been accomplished without the support of my colleagues: Dr. Hassan Ghassemi-Armaki; who provided full support for the testing facilities, equipment and all necessary components; Dr. Blair Carlson, the sponsor for the study and Dr. Jun Zhou for the time of reviewing the reports and providing the valuable feedback.

Finally, to my wife, Dr. Shixiang Gao and my children: Patricia, Nancy and Kevin for continued support and encouragement.

Xiaobao Huang

# PREFACE

Automotive industry is experiencing an important transformation from a heavy steel box to a combination of sheet metal, high strength low alloy, high strength steel, advanced high strength steel, ultra-high strength steel, Boron/Martensite, AL 5000/6000, aluminum/high strength aluminum, Mg and Carbon fiber reinforced plastic/composites. This change in basic materials will require advanced fastening technology in manufacturing process to provide quality connection in between different materials. Adhesive joint can provide such connectivity with low cost, easy applicability, continued structural support with reliability and longevity.

Testing and providing quality adhesive joints become crucial tasks in terms of fatigue data for certain adhesive material and configuration of the joint. The detection of adhesive failure and cycles is the main focus for the testing community and currently only a few methods can provide reliable results, but with high cost of testing equipment and components such as high-speed cameras and associated software.

The current study aims at the following criteria: low cost, easy to apply, reliable, scalable with less training in different regions around the world. This study took a different approach in utilizing an accelerometer with Fast Fourier Transform (FFT) process the time domain data and obtain frequency domain data, then transform into a new dimension for data analysis and obtain reliable results in identifying different stages of joint failure.

ABSTRACT

AMPLITUDE METHOD TO DETECT DEBONDING FOR STACK BOND ADHESIVE

by

XIAOBAO HUANG

Adviser: Gary Barber, Ph.D.

A numerical method was developed to detect debonding (crack initiation) condition during fatigue testing of an adhesive joint with thin steel sheets in standard configurations of coach peel and lap shear specimens. The goal is to establish the relationship between the sample's vibration behavior and initial failure condition, this relationship can be used to develop fatigue S-N curves for the adhesive under geometrical configurations of either coach peel or lap shear specimens. This method focuses on the continued monitoring of the specimen's vibration status by transferring the wave form data (in time domain) to a Fast Fourier Transform (FFT) process and obtaining frequency and amplitude data (in the frequency domain), this data is then processed to identify the critical events such as debonding (crack initiation), crack propagation and total failure with associated cycle counts for each event. The amplitude output files were used to analyze the progression of different stages of failure for the samples under cyclic loads. Video analysis of failure modes was utilized to identify the different types of damage matching the cycle count based on time scale (frames) for each stage. ANSYS models were generated to provide supporting evidence in terms of change in natural frequencies

and amplitude due to change of internal stiffness of the specimens. Certain mode shapes were analyzed to gain confirmation of the relationship between mode shape, amplitude, and initial failure of the samples.

TABLE OF CONTENTS

LIST OF TABLES

LIST OF FIGURES

# LIST OF ABBREVIATIONS

| | |
|---|---|
| da/dN | Derivative of crack length subject to fatigue life, a=length of crack, N = fatigue life (in cycles) per Paris-Law. |
| ΔK | micro-movement on stress concentration factor K, per Paris-Law. |
| S | Stress in MPa |
| N | Fatigue life, in cycles |
| $\mathcal{E}$ | strain of material |
| $G_{th}$ | Fracture toughness, a combination of $G_n$ (in tension) and $G_s$(in shear) |
| **u** | displacement vector |
| **U** | Eigenvector |
| ω | Natural frequency |
| λ | Eigenvalue |
| **K** | Stiffness matrix |
| **M** | Mass matrix |
| D | Damage of test sample under cyclic load |
| $N_{f0}$ | Number of cycles bore crack initiation |
| $N_{f1}$ | Number of cycles at the crack initiation |
| e | Eccentricity between ext. load axis and adhesive surface |
| $e_c$ | Critical eccentricity where adhesive debonding occurs. |

# CHAPTER ONE

# INTRODUCTION

Adhesively bonded joints have been applied in the automotive industry for the past few decades due to their advantages such as higher fatigue resistance, light weight, capability of joining dissimilar materials, good energy absorption and high torsional stiffness for overall body structure. They also provide an effective seal against noise and vibration with a low cost. There exists the challenge of defining the fatigue characteristics of adhesive joints under cyclic loading conditions and conventional methods have limitations in detecting the crack initiation of a bonded joint.

## 1.1 Adhesive failure dections

In order to fully understand the behavior of an adhesive under fatigue loading conditions, multiple methods [1] have been developed to predict the fatigue life of bonded joints such as: stress-life (S-N) method based on total strength to total life, strain-life (Ɛ-N) similar to strength-life but monitoring of the strain vs. cycles, continuum fracture mechanics based on the Paris Law ($da/dN=C(\Delta K)^m$) where the right side of the equation can be different forms such as strain energy release rate, compliance form (displacement vs. load), stress-intensity factor and other variables. The process of adhesive joint failure for a pure shear (lap shear sample) can be described as: during the load transfer from one sheet to another, the adhesive layer continues to absorb energy (in the form of stress or strain) until a critical energy level is reached, $G_{th}$, then the bond starts to fail in the form of micro cracks developed inside the adhesive layer which is commonly interpreted as crack initiation. The joint continues to transform external energy into deformation where crack length continues to grow (crack propagation) until the crack length reaches a critical length causing general failure due to de-stabilization of the joint. For the case of a coach peel sample, the debonding can occur before any internal crack initiated due to the pure tension load condition in some cases when the entire width of the specimen debonds and in other cases the initial crack occurred simultaneously with the debonding.

The Cohesive zone model (CZM) [2] is widely used in describing fracture mechanics where fracture formation at the crack tip due to external force exceeds the cohesive traction (force). Under cyclic loading, the cracks will initiate at the point where external force (in general tension, shear or mixed) exceeds the material's strength respectively and follows a straight line (simplified model) with the total displacement at the bottom of a triangle (formed by total displacement and total strength). As the cracks grow under each cycle of load, the accumulation of damage (propagation of cracks) on the adhesive causes gradual degradation of material properties which then leads to global yield and then the joint fails by cohesive failure in the adhesive.

Jen and Ko [3] studied the effect of adhesive dimensions on the fatigue strength of adhesively bonded aluminum single lap joints (SLJ)s and found that the fatigue resistance decreased as the overlap length increased except for the specimens with an adhesive thickness of 0.5 mm. From finite element analysis (FEA), they concluded that the interfacial peeling stress (debonding) was the main driving force of the fatigue failure of the SLJ's. Gao and Yue [4] performed a special bending fatigue experiment to investigate the fatigue behavior of polyethylene methacrylate in an adhesive assembly. From experimental data and FEA, they derived a local stress law for predicting bending fatigue lifetime. Using curve fitting of the experimental data, they established a relationship between the maximum tensile stress and the number of cycles.

Gomatam and Sankara [5,6] studied the effects of stress state and cyclic parameters, they found a significant effect of the stress state and cyclic waveform type on the fatigue strength of the joints. They also observed that lowering the cyclic load frequency reduced the fatigue life.

### 1.2 Damage, Monitoring and failure

Graner Solana et al. [7] used an elastoplastic damage model to predict the fatigue lifetime, which is similar to the Paris Law format. They carried out low cycle fatigue tests to determine the damage variable, D, as a function of the number of cycles. Damage was evaluated using the decrease in stress range during fatigue life cycles during a constant displacement amplitude test [8,9].

Quaresimin and Ricotta [10] studied the evolution of life of the joint which was spent in the nucleation of one or more cracks. They found that the duration of the nucleation process was increased from 20% to 70% of the joint life. For crack monitoring, Zhang et al. [11] developed a back-face strain technique to detect fatigue crack initiation in SLJs. From experimental measurements, they found that fatigue crack initiation lives at different stresses compose a greater proportion of the total fatigue life as the stress decreased. Crocombe et al. [12] studied the fatigue damage evolution in adhesively bonded joints using the back-face strain technique. From the results of the fatigue tests, they found that there was an initiation phase of about half the total fatigue life of the joint.

Bernasconi A. et al. [13] studied adhesively bonded single lap joints using the Back-Face (BF) strain technique based on distributed strain sensing by Optical Backscatter Reflectometry (OBR) to monitor Fatigue Crack Growth (FCG) in adhesive joints between Carbon Fiber Reinforced Polymer (CFRP) adherends and compared their performance with micro computed tomography ( μ CT) observations. The study concluded that the available spatial resolution of the used OBR system limits the possibility of accurately defining the actual crack size for damage smaller than 2 mm. On the other hand, for sufficiently large damage (6–6.5 mm), this method was able to detect the size and monitor the actual dimension of the cracks with good accuracy.

### 1.3 Crack related change in natural frequencies

Barad, Rizos et al. [14,15] applied the frequency-based method to detect the change in natural frequency of a cantilever beam by embedding a notch as an artificial crack, modeling the crack point with a spring stiffness K, evaluating the natural frequency of modes, location of the crack and size of crack to determine the relationship between crack depth and changes in frequency. They found that the stiffness was reduced when crack depth increased. Khatir et al. [16] used changes in experimentally measured frequencies and particle swarm optimization to identify the crack in a beam-like structure. They observed that for a steel beam with 0.7 m length, cross section area 0.0001 $m^2$, Young's modulus 200 GPa, post installed crack of 3 mm depth at cross section (30% loss rigidity) the measured mode 3 natural frequency was decreased to 296 Hz as compared to an undamaged section measurement of 307 Hz.

### 1.4 Summary of current detection procedures

Various methods were developed to predict fatigue life of a joint:

1- Paris law format which monitors change in crack length with stress intensity factor, or strain energy release rate during damage progression.

2- Cohesive zone method which monitors the plastic energy change with traction separation by the surface stress change from external force.

3- Back face strain gauge method by Sadeghi et al.[17] to monitor the elongation of a specimen to compare material property limits.

4- Digital image correlation (DIC) method by Sawada et al. [18] which uses high speed cameras to monitor adhesive edge movement and identify crack initiation by calculating the second derivative of wave form.

5- Frequency method which is used to verify the internal damage of a structural beam with an artificial crack by tracking the change in natural frequency due to change in stiffness.

Among all methods above, except #4 (DIC) which can accurately identify the cycle at crack initiation, every method is based on linear elastic fracture mechanics which focuses on the post crack development or crack propagation. With the DIC method, multiple cameras are required from different angles to capture all edges of a specimen, the crack generally initiates from external stresses/strains. The limitation is that once the first crack initiates inside the edge, the result may not be accurate.

The objective of the current study is based on #5 above (using the frequency method to detect the effect of an embedded crack in a beam) with improvements:

A- No pre-embedded crack is required, so that the fatigue life from $\boldsymbol{N_{f0}}$ to $\boldsymbol{N_{f1}}$ can be obtained.

B- To process acceleration (wave form) data with FFT in real time, to record and evaluate changes in natural frequencies and associated amplitudes, analyze and identify the pattern change in terms of amplitude values in order to pinpoint the damage in different stages, along the loading cycle axis

C- Enhance the testing process by monitoring sample's internal change of stiffness and not rely on visual monitoring a sample from #4 above (detecting crack initiation only on outside edges). This is important for a joint with crack initiation or debonding not starts at the corners of the sample.

This study will make it possible to detect fatigue life (in term of loading cycle count) of a specimen from uncracked to crack initiation ($\boldsymbol{N_{f1}}$) without embedding an artificial crack and correctly identify the fatigue life. Further, this method can also determine the cycle counts at each stage of damage: crack initiation (or debonding), crack propagation (mostly involved in cohesive damage progression) and final failure (separateion of sample).

## 1.5 Amplitude monitoring concept

The amplitudes associated with natural frequencies of an object during vibration are effect of changes of internal stiffness. When adhesive between two steel sheets starts debonding (crack initiation), the assembly stiffness decrease and this will be reflected by change in certain natural frequencies and associated amplitudes. Monitoring or tracking the change in natural frequencies under a dynamic loading system can be difficult due to a non-linearity effect, where the grips of the loading machine slip (even with automatic compensation by the machine), the system becomes non-linear. A non-linear system is subjected to super harmonic and sub harmonic conditions where all system frequencies and natural frequencies will generate additional frequencies as 3f, 5f, 7f.... and 1/3f, 1/5f, 1/7f… and the entire system becomes noisy with many system harmonics. Filtering out all the noise from the system is much harder and costly from a resource point of view. Compared to tracking of natural frequencies, tracking amplitudes can be relatively easier.

1- detect the debonding (crack initiation – adhesive failure) during cyclic loading of a sample and the crack propagation;

2- detect the cohesive damage, its propagation and the substrate material participation of load resistance (in bending);

3- final stage of damage with total failure identified as complete separation of a sample.

During each of the failure stages, the coresponding damage of each type was observed, and cycle counts for each damage were identified (by video analysis of failure progression of the sample) and subsequently by comparison between monotonic load-displacement diagram and the amplitude-FFT Block diagram.

Finite element analysis (FEA) models were generated to simulate the crack initiation and its effect on amplitude value change in different mode shapes and in each direction (in X, Y, Z axies) of vibration. Such FEA model simulation provided confirmation of spikes in value of amplitude in case of stiffness drop for the sample. MTS fatigue machine provided additional indication on each stage of failure by reaction load values vs. cycle count.

# CHAPTER TWO

# THEORIES AND ANALYSIS MODELING

## 2.1 Fundamentals and Theories (Newton's second law)

Newton's second law describes the equation of motion for an undamped mass-spring system as:

$$\mathbf{M}\ddot{\mathbf{u}} + \mathbf{K}\mathbf{u} = F \tag{1}$$

where M and K are, respectively, the mass and stiffness matrices of the structure, **u** is the nodal displacement vector, **ü** the nodal acceleration vector and F the nodal force vector. To determine the natural frequency, it is assumed that the system produces harmonic oscillations under free vibration, or F = 0. Thus,

$$\mathbf{u}=\mathbf{U}e^{i\omega t} \tag{2}$$

where **U** is the amplitude of nodal displacement also called Eigen vector, i = $\sqrt{-1}$, $\boldsymbol{\omega}$ the frequency of the harmonic function and t the time. Therefore, Eqn. (1) becomes:

$$(-\omega^2\mathbf{M}+\mathbf{K})\mathbf{U}e^{i\omega t}=\mathbf{0} \tag{3}$$

For a non-trivial solution for **U** to exist, the determinant of the coefficient matrix must be zero. Thus,

$$\|\mathbf{K}-\lambda\mathbf{M}\|= 0 \tag{4}$$

where $\boldsymbol{\lambda} = \boldsymbol{\omega}^2$ ($\boldsymbol{\lambda}$ is the Eigen value), and ‖. ‖ = det (. ) is the determinant of a matrix. It is called the characteristic equation and can be used to determine the vibration system's natural frequencies and subsequent modes. The relationship (4) indicates when stiffness matrix **K** changes due to internal damage, the change in $\boldsymbol{\lambda}$ can be determined since **M** is constant.

## 2.2 Fast Fourier Transform

Fourier Transform is a mathematical transformation between a signal in time domain and a signal in frequency domain. Assuming a time domain function f(t) to be transformed by Fourier transformation, the forward transformation takes the format:

$$\hat{f}(\xi)=\int_{-\infty}^{\infty} f(t)e^{-2\pi i\xi t}dt \tag{5}$$

The $\hat{f}$ is the transformed function in frequency domain; f(t) is the original time domain function; $\xi$ is a real number.

Developed in 1965 by Cooley and Tukey, a Fast Fourier Transform (FFT) was proven to be more advanced in computing Discrete Fourier Transform (DFT) of a sequence or its inverse (IDFT). The DFT is obtained by decomposing a sequence of values into components of different frequencies. This operation is widely appplicable for its capability of obtaining output of specitrum data (in frequency domain) from wave from (time domain) data. FFT can perform fast transformations by factorizing the DFT matrix into a product of sparse (mostly zero) factors thus to reduce the complexity of computing the DFT from $O(n^2)$ to $O(n \log n)$ where n is the data size.

Let $x0, \ldots\ldots, xn-1$ be the complex numbers. The DFT is defined by the formula:

$$X_k = \sum_{m=0}^{n-1} x_m e^{-\frac{i2\pi km}{n}} \qquad (6)$$

$k = 0, \ldots, n-1,$

where $e^{\frac{i2\pi}{n}}$ is a primitive n'th root of 1.

Evaluating this definition directly requires $O(n^2)$ operations: there are n outputs *Xk*, each requires a sum of n terms. An FFT can compute the same result in $O(n \log n)$ operations. Consider the count of complex multiplications and additions for n=4096 data points. DFT's sums directly involves $n^2$ complex multiplications and $n(n-1)$ complex additions, from that the $O(n)$ operation can be saved by eliminating trivial operations such as multiplications by 1, leaving about 30 million operations. Using Cooley-Tukey algorithm, for n with a power of 2, can compute the same result with only $(n/2)\log_2(n)$ complex multiplications and $n \log_2(n)$ complex additions in total of 30,000 operations realizing an overall improvement from $O(n^2)$ to $O(n \log_2 n)$.

2.3 Data transfer from time domain to frequency domain before crack initiation

A typical solid block's vibration wave form (in time domain) can be described as:

$$F(t) = A \cos(\omega t) \qquad (7)$$

After two consecutive derivitaves:

$$\partial^2 F/\partial t^2 = -A\omega^2 \cos(\omega t) \quad (8)$$

$\partial^2 F/\partial t^2$ is the acceleration (vector) by difination. This means that the acceleration vector is the same vector as positioning vector (in time domain) with a negative scaler. As input values (in time domain) feed into an accelerometer, thru FFT process, this time domain data is being processed to obtain spectrum data (in frequency domain). Therefore a direct link between an object's vibration data and it's spectrum output data is established.

## 2.4 Data transfer from time domain to frequency domain after crack initiation

A cracked block vibration wave form: Since the $\omega$ is a time dependant virable ($\omega$ (t)) due to the fact that Stiffness matrix K is changing during the damage process, the acceleration vector becomes:

$$\frac{\partial^2}{\partial t^2}(A\cos(\omega(t)\cdot t)) = A((t\,\omega'(t)+\omega(t))^2\left(-\cos\left(t\,\omega(t)\right)\right) - \sin\,(t\,\omega(t))(t\,\omega''(t) + 2\omega'(t))) \quad (9)$$

The new acceleration vector (9) as the input data for FFT process becomes much more complicated. The output spectrum plot's noise level can get very high due to this input plus all system harmonics generated according to the non-linearity.

## 2.5 Defining debonding, crack initiation and crack propagation

There are multiple types of failure in an adhesive joint:

1. Adhesive failure, defined by the separation between the adhesive layer and the base metal surface. This happens when external force exceeds the bond strength between the metal surface and the adhesive layer. See Figure 1.

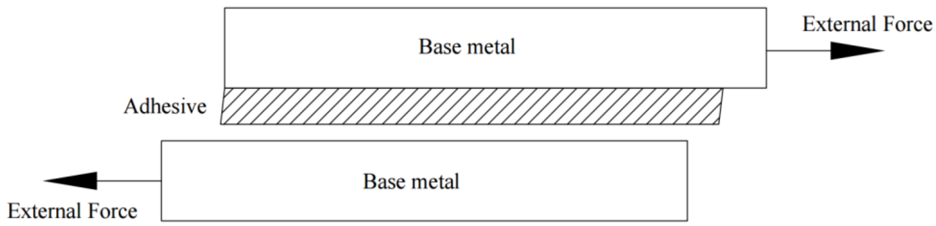


**Figure 1. A typical adhesive failure**

2. Cohesive failure, defined by the failure of adhesive layer, the crack splits the adhesive layer so both metal surfaces have left over adhesive material. This happens when external force exceeds the cohesive strength of the adhesive material, at the same time the bond strength between metal and adhesive is stronger than the cohesive strength. See Figure 2.

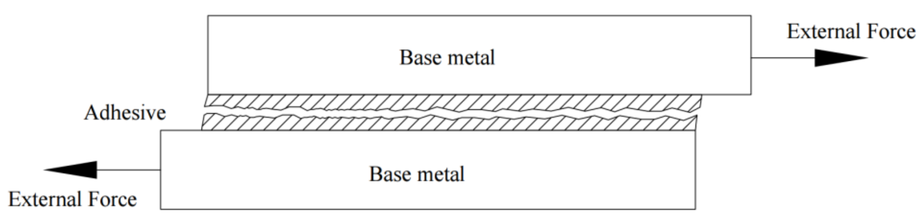


**Figure 2. A typical cohesive failure**

3. Combination failure model with adhesive and cohesive failure at the same time, although it seems this failure occurs coincidantly, it is the author's believe that theadhesive failure starts the general failure, the crack migrates into area where internal defect of adhesive and splits the adhesive layer causing the cohesive damage. See Figure 3.

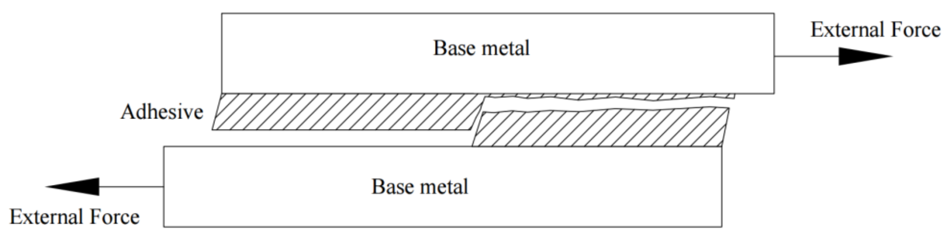


**Figure 3. A combination (adhesive and cohesive) failure**

4. Substrate material failure where the base metal fails before any of the adhesive material starts failure, this topic is not the scope of current study.

## 2.6 Damage analysis of CP sample under monotonic load condition

The damage analysis of test samples for Coach Peel under monotonic loading condition can be useful in determining the type of failure at each stage of load-displacement diagram.

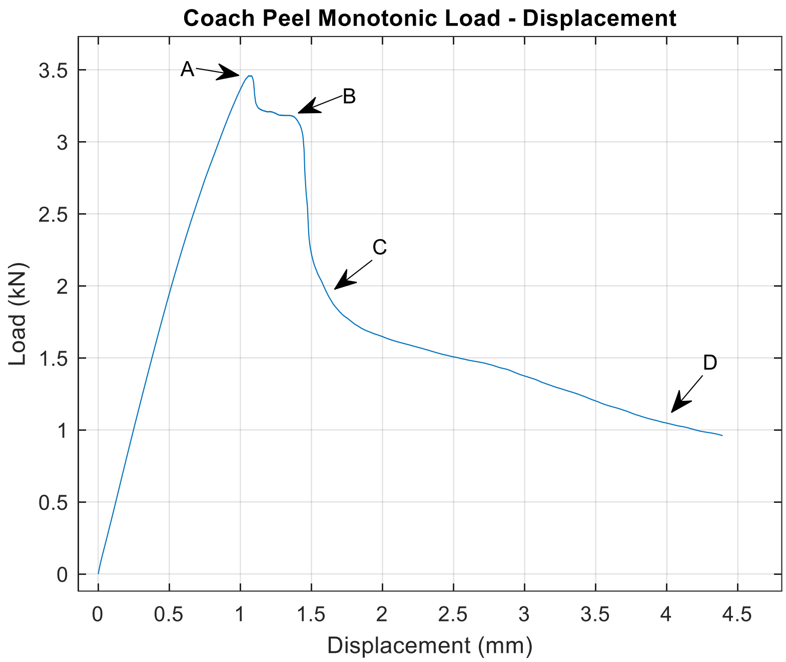


**Figure 4. Load-displacement diagram for coach peel sample**

As shown on Figure 4, the Coach Peel sample's diagram can be divided into 4 parts:

0-A: An almost linear relation is observed as displacement increase with the load.

At point A: the onset of peeling initiated (debonding). This is the beginning of the adhesive failure (debonding or crack initiation) as determined by visual observation. During this process the force dropped initially due to loss of system stiffness in terms of bonded area. Then the curve flattened indicated the pull apart steel sheets with continued increase in displacement. Material separation (crack propagation, steel sheet and adhesive debonding) continued to point B.

At point B: the failure mode transitioned from adhesive failure to cohesive failure. This is the point the cohesive resistance combined with the steel sheet's bending capacity were in effect. During the cohesive failure the load value dropped significantly with almost no displacement. This is partially due to the moment arm of bending (the distance from the pulling point to the crack propagation point) continued increasing with constant force setting for the machine, and the remaining bonded area continued to shrink therefore with less resistance. Adhesive material separation with (crack propagation) combined with steel sheets' deformation continued until point C.

At C: the adhesive separation (cohesive failure) continued. The combined cohesive resistance with the steel sheet bending worked together till point D where the sheets separated completely. From point C to D the force reduced linearly with displacement till reaching the machine preset limit.

## 2.7 Damage analysis of LS sample under monotonic load condition

For a typical Lap Shear sample, shown in Figure 5,

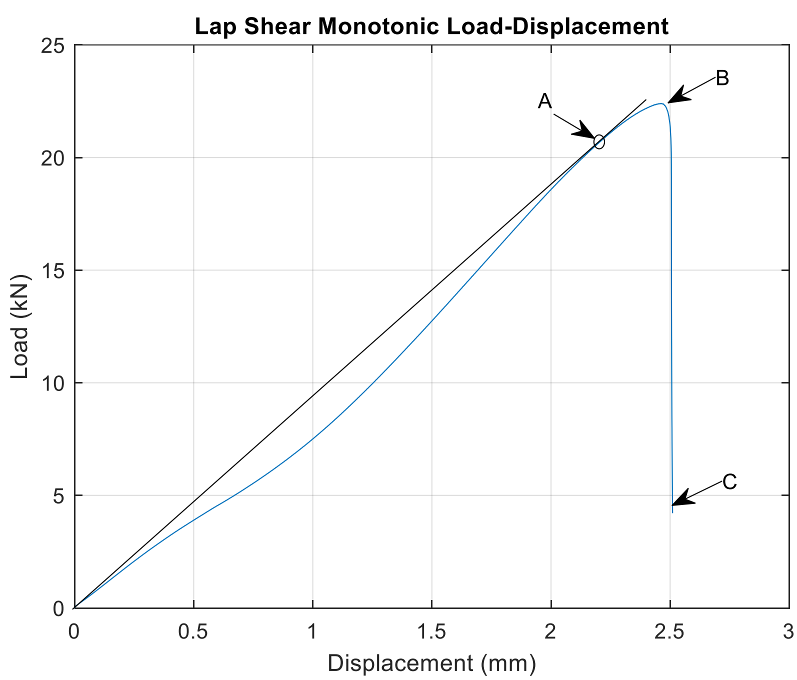


**Figure 5. A typical las shear sample load-displacement diagram**

the load-displacement diagram has the following characteristics:

0-A: The load and displacement curve followed a slight downward curve line indicating a strain softening to around 1mm displacement, then experienced strain hardening towards “A”.

At A: The curve transitioned from concave to convex, indicating a change from strain hardening to strain softening; Material plasticity took effect after “A” as the shear stress increased until point “B”.

At B: As the plastic deformation continued with increased load due to the increase of eccentricity e (see Figure 18), the edges of adhesive experienced combined stress of shear and moment, when this stress reached to a critical point ($e_c$), the adhesive failure (debonding) started. This failure in adhesive quickly triggered the cohesive failure due to the loss of adhesive area to resist the external force. As the adhesive and cohesive failure occurred at almost the same time, the applied external stress exceeded the strength of the system, which is composed of combined adhesive and cohesive strength, the general failure occurs with the displacement curve dropping sharply with no displacement due to the machine preset load limit.

Lap shear sample failure is always sudden with no warning except some permanent deformation due to bending at the corners which indicates adhesive (and cohesive) failure accumulation separately on opposite corners (never mixed).

As shown in Figure 5, the non-linear elastic properties can be attributed to the study completed by Mihai et al [20] based on the material shear modulus (10) and Poison function (11) specified as:

$$\mu(a,k) = \frac{\sigma_{12}}{ka^2} \qquad 10$$

$$V^{(H)}(a) = -\frac{\ln \lambda(a)}{\ln a} \qquad 11$$

where $a$ >0 is the stretch parameter, k is the ratio per Figure 6, $\sigma_{12}$ is the shear stress in the cuboid, $\lambda(a)$ is the principal stretch. The superscript (H) indicates the strain tensors defined as Hencky [21] method (logarithmic or true).

Both shear modulus and Poinson functions contribute to the non-linearity of the system as they are functions of deformation $a$.

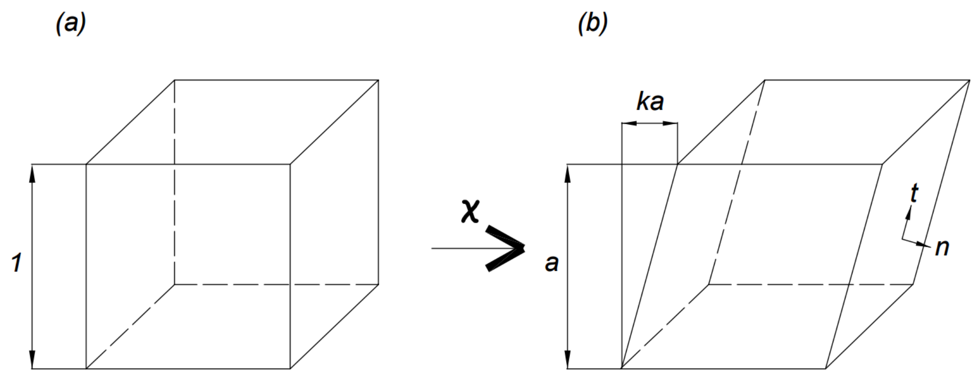


**Figure 6. Cuboid (a) deformed by simple shear superposed on axial stretch (b), showing the unit normal and tangent vectors on an inclined face.**

## 2.8 Finite Element Model (FEA) of CP and LS samples

The impact on amplitude values by an internal crack in adhesive layer is shown on Table 1. The values in column 3, 4 and 7 corresponding to X, Y, Z of each mode are Directional Displacements (DD). They are relative values to describe the deformation shape (not in absolute dimensions). They can be defined as: when the sample is deformed into a particular mode shape and released, it will oscillate between the initial deformed shape and the negative of the initial deformed shape at a frequency ω which is the natural frequency. Values in column 3 represent non cracked shape, values in column 4 are results from an embedded crack in adhesive layer, it has a semi elliptical shape with 2 mm in length. The values in column 7 are results from the crack length grew from 2 mm to 3 mm. The highlighted values in columns 6 and 9 are percentage increase of DD in Y direction for mode 3 and 6, indicating the effect of loss of stiffness due to the crack's present.

The Associated Finite Element Modeling with relative mode shapes are shown in Figure 7 and Figure 8.

**Table 1. Coach Peel Sample Directional Displacement Value Change by Crack's Present and Growth**

| Modes | Direction | No Crack | Crack Embed 1 | Up/Down | % Change | Crack Embed 2 | Up/Down | % Change |
|---|---|---|---|---|---|---|---|---|
| Mode 1 | X | 150.13000 | 151.71000 | ↑ | 1.05% | 152.16000 | ↑ | 1.35% |
| | Y | 1.25410 | 1.25630 | ↑ | 0.18% | 1.24990 | ↓ | -0.33% |
| | Z | 0.10841 | 0.10845 | ↑ | 0.04% | 0.10771 | ↑ | -0.65% |
| Mode 2 | X | 195.83000 | 199.99000 | ↑ | 2.12% | 200.36000 | ↑ | 2.31% |
| | Y | 1.68720 | 1.68470 | ↓ | -0.15% | 1.66870 | ↓ | -1.10% |
| | Z | 265.88000 | 271.61000 | ↑ | 2.16% | 271.70000 | ↑ | 2.19% |
| Mode 3 | X | 167.45000 | 168.58000 | ↑ | 0.67% | 168.48000 | ↓ | 0.62% |
| | Y | 3.29260 | 163.18000 | ↑ | 4855.96% | 163.50000 | ↑ | 4865.68% |
| | Z | 0.46689 | 0.46905 | ↑ | 0.46% | 0.46970 | ↓ | 0.60% |
| Mode 4 | X | 187.43000 | 187.43000 | - | 0.00% | 186.94000 | ↓ | -0.26% |
| | Y | 4.86430 | 4.76780 | ↓ | -1.98% | 4.69130 | ↓ | -3.56% |
| | Z | 0.84219 | 0.83221 | ↓ | -1.19% | 0.82421 | ↓ | -2.13% |
| Mode 5 | X | 152.54000 | 153.40000 | ↑ | 0.56% | 151.76000 | ↓ | -0.51% |
| | Y | 286.38000 | 297.52000 | ↑ | 3.89% | 299.82000 | ↑ | 4.69% |
| | Z | 0.83212 | 0.84798 | ↑ | 1.91% | 0.83705 | ↓ | 0.59% |
| Mode 6 | X | 304.26000 | 303.96000 | ↓ | -0.10% | 303.27000 | ↓ | -0.33% |
| | Y | 40.86800 | 48.33200 | ↑ | 18.26% | 50.70500 | ↑ | 24.07% |
| | Z | 11.32000 | 11.62600 | ↑ | 2.70% | 11.78200 | ↑ | 4.08% |

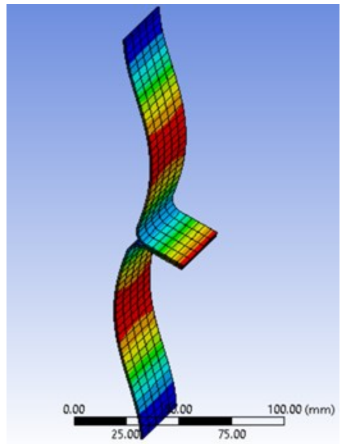


**Figure 7. Coach peel sample mode 3 with crack in adhesive layer**

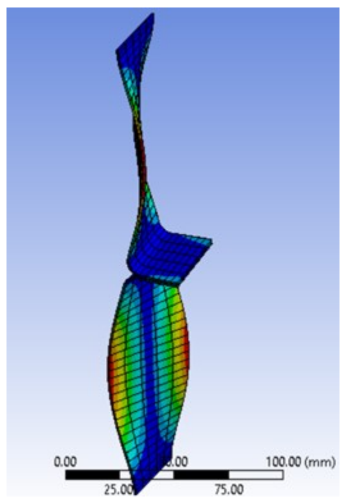


**Figure 8. Coach peel sample mode 6 with crack in adhesive layer**

Evaluation of Table 1 values (for CP) yields following observations:

1. When an artificial crack is embedded in the adhesive layer, with the increase of size of the crack from 0 to 2 mm, a progressive movement of directional displacement values for each mode can be observed. Depending on the load

direction and mode shape, the damage by the present of a crack can cause directional displacement values to change (up or down).

2. The large values change occurred where the external load direction matches the direction of the most damaging mode shape by the crack. As shown in Table 1 and Figure 9, mode 3 in Y direction produced the directional displacement value increased by 4856%.
3. Value changes in other directions under each mode tend to be in low percentage and stayed that way with increasing of crack length, never mixed (switch sign).

For Lap Shear sample, FEA model revealed similar results shown in Table 2, Figure 9.

**Table 2. Lap Shear Sample Directional Displacement Value Change by crack's Present**

| Modes | Direction | No Crack | Crack Embed | Up/Down | % Change |
|---|---|---|---|---|---|
| Mode 1 | X | 1.4922 | 1.4922 | - | 0.00% |
| | Y | 0.0198 | 0.01981 | ↑ | 0.05% |
| | Z | 0.00227 | 0.00227 | - | 0.22% |
| Mode 2 | X | 2.5211 | 2.5207 | ↓ | -0.02% |
| | Y | 0.04831 | 0.04834 | ↑ | 0.06% |
| | Z | 0.17549 | 0.17525 | ↓ | -0.14% |
| Mode 3 | X | 1.8077 | 1.8081 | ↑ | 0.02% |
| | Y | 0.08925 | 0.08924 | ↓ | -0.01% |
| | Z | 0.01325 | 0.01325 | - | 0.02% |
| Mode 4 | X | 1.9664 | 1.9669 | ↑ | 0.03% |
| | Y | 0.06967 | 0.06969 | ↑ | 0.03% |
| | Z | 0.01669 | 0.01667 | ↓ | -0.10% |
| Mode 5 | X | 3.1054 | 3.1066 | ↑ | 0.04% |
| | Y | 0.09807 | 0.09806 | ↓ | -0.01% |
| | Z | 0.0761 | 0.11246 | ↑ | 47.77% |
| Mode 6 | X | 3.0255 | 3.0263 | ↑ | 0.03% |
| | Y | 0.12067 | 0.12069 | ↑ | 0.02% |
| | Z | 0.12312 | 0.12318 | ↑ | 0.05% |

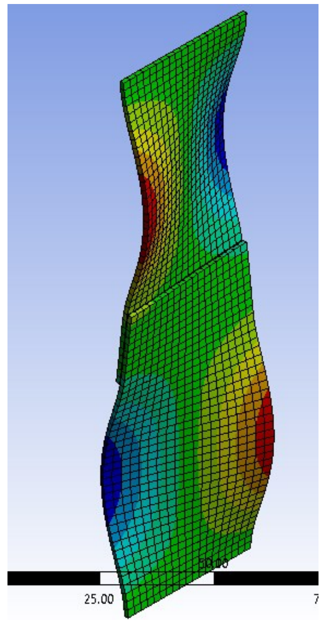


**Figure 9. Las shear sample mode 5**

Evaluation of Table 2 and Figure 8 with the following observations derived:

1. The present of a crack in adhesive will make directional displacement values in different mode and direction change.
2. The largest value change coincides with the most damaging shape in the same effect by the external force, in this case the twist of the sample causing the bending at the end of adhesive (edge) where the sample tends to split. The change in value is the highest percentage (47%) compared to all other value changes.
3. The values change in other mode and direction tend to be in low percentage and stay that way.

Discussion

The mode shape corresponds to external force with maximum damage to the sample due to embedded crack will have the stiffness value decrease due to loss of resistance area. Transversely, the stiffness seen increases due to the gap being generated between material blocks, the moment of inertia increases due to the gap's expansion.

For the directional displacement values change in the FEA models under Coach Peel sample, the increase in value corresponding to certain mode in the direction of external force can be explained as the increase damage would reduce the stiffness for the internal structure, there will be less material participate in load resistance activity therefore the displacement increases. As for Lap Shear sample joint, the mode shape corresponding to the maximum damage due to the crack present would generate a large increase in directional displacement values, as shown in Figure 8 where the bending of the joint per mode shape and the direction of "Z" would be the most damaging orientation.

FEA modeling as a convenient tool (for simulation) can help in visualizing the change in values of directional displacement in X, Y and Z directions within each mode due to a crack's present. The reason to select this metric for damage monitoring is that the model of a specimen consists of a few thousands of elements with each element consisting of 8 corners (for rectangular element) and 24 degrees of freedom for each (18 for triangle elements). The stiffness matrix will contain a total number in tens of thousands of items squared values ($n^2$). It is hard to evaluate this massive numbers and track the changes of each. Similarly, Eigenvector will be in the tens of thousands (n by 1 matrix) numbers and still very hard to track and evaluate. The peak value change for directional displacement presents a feasible option in evaluating the effect of internal damage by comparing the pre-crack and post-crack top values change, such as Table-1 and 2.

## 2.9 Summary

Based on the fundamental theories and data transformations between time domain and frequency domain, the intrinsic relationship among the stiffness, vibration amplitude corresponding to external force and internal damage can be seen as a tool to develop a damage detection mechanism. Utilizing this relationship can be beneficial for engineering of the joint design with S-N curve development and potentially other applications such as continued monitoring the vibration status for critical components. The fact that most of the amplitude values movement are small in percentage with only one to be extremely high, makes the detection of the spike possible and to be a reliable metric for this application.

# CHAPTER THREE

# EXPERIMENT AND TESTING

## 3.1 Load test specimen configuration for Coach Peel and Lap Shear

The sample test specimen configuration and geometries are shown in Figure 10. The adherent material is DP590 bare steel sheet with thickness of 1.1 mm. The thickness of adhesive is 0.2 mm per production requirement.

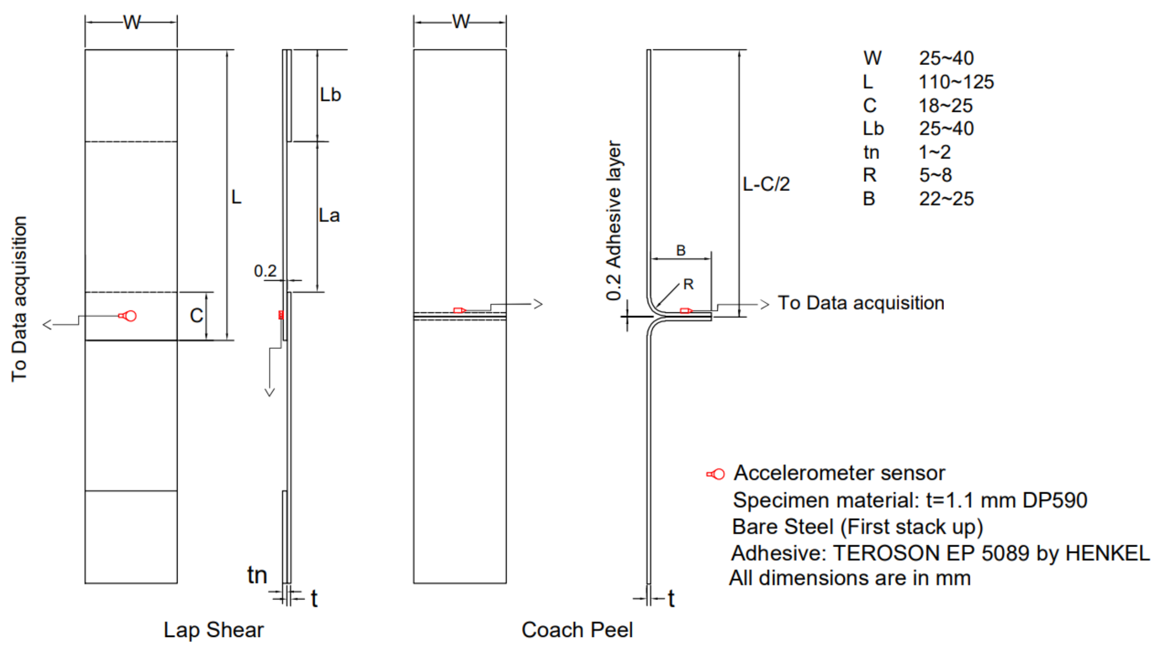


**Figure 10. Geometries of testing samples**

## 3.2 Adhesive material properties

The adhesive material is manufactured by Henkel® Adhesive Technologies, type: TS-5089 with stress-strain curve shown on Figure 10. The detailed material specification is shown in Table 3. The application of adhesive is in room temperature, the curing process is 170º C for 25 minutes oven baking.

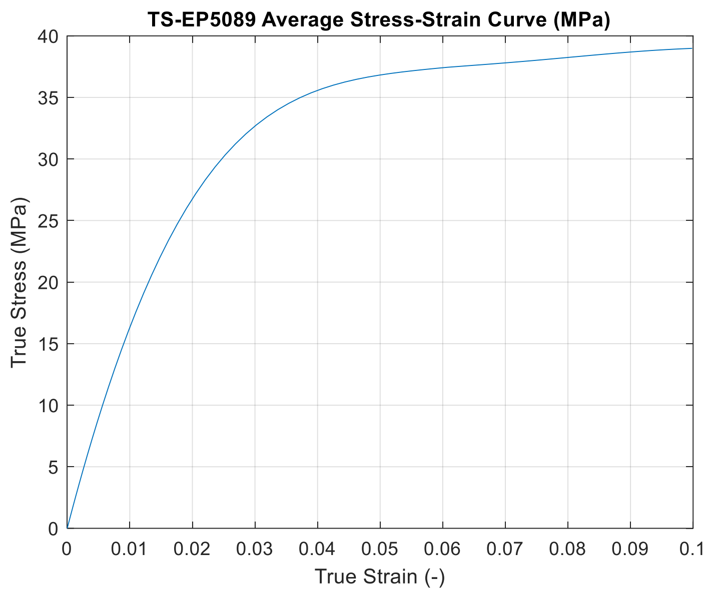


**Figure 11. Adhesive stress-strain curve by Henkel®**

**Table 3. Adhesive material properties by Henkel®**

| | |
|---|---|
| (Typical Test Results) | |
| Uncured | |
| Color | Purple |
| Density | Approx. 1.2 g/cm³ |
| Consistency pasty | Consistency pasty |
| Solids | > 99 % |
| Viscosity (DIN 54458) | 250 Pa. s |
| Equipment | Plate/Plate 25 mm Ø |
| Temperature | 45 °C |
| Deformation | 10% |
| Frequency | 10 Hz |
| Cured (25 min, at 175 °C) | |
| Material Data: | |
| E-Modulus | 1.6 GPa |
| Tensile strength | 35 MPa |
| Elongation at break | 10% |
| Poisson rate | 0.4 |
| Shear strength (DIN EN 1465) | > 20 MPa |
| Layer thickness | 0.2 mm |
| Bonding area | 25 x 10 mm |
| Substrate | HDG/EGS 0.75 mm |

**Table 3. - Continued**

| | |
|---|---|
| Impact-Peel | > 25 N/mm |
| Salt spray test | No loss of adhesion |
| (35°C, salt solution 5%, 1,000 hours) | No corrosion |
| In service temperature range | -40 to 90 °C |

## 3.3 Fatigue test equipment (MTS) and test control parameters

For load test equipment, the MTS 858 vibration tabletop system was used. Equipped with 647 Hydraulic wedge grips, this loading system has a load range of 0.3 kN ~ 20.0 kN force with mean value of 0.3~10.0 kN sinusoidal waves and applied frequency range of 1~6 Hz. For the current study the sinusoidal wave is regular shape with load control (constant load value) setting. Figure 12 shows the testing samples set up and Figure 13 shows the control panel screen for testing parameters.


**Figure 12. MTS 858 Tabletop System, Coach Peel and Lap Shear Samples Set Up**

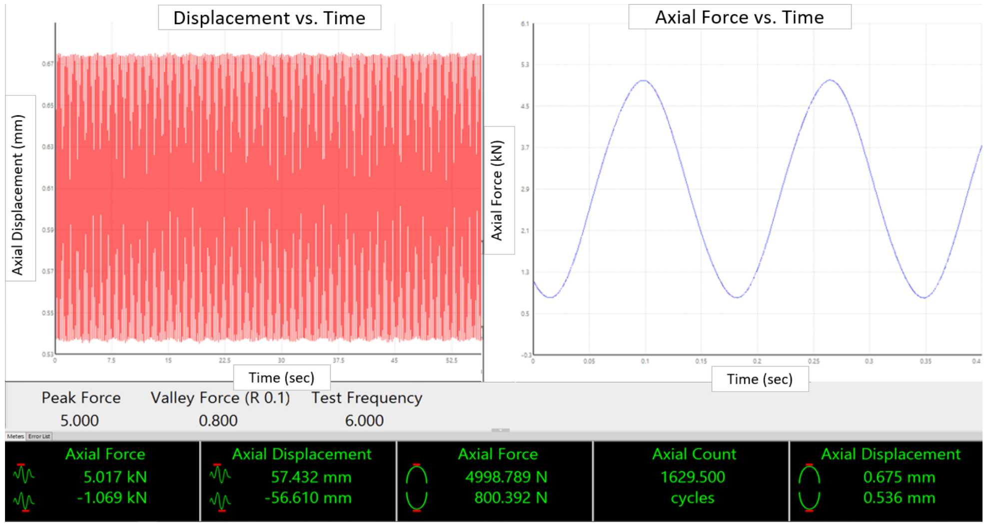


**Figure 13. Control Screen of MTS 858 Vibration System**

3.4 Data acquisition hardware

Shown in Figure 13, the system includes a PC with Windows 10 Pro OS; The data acquisition box is Digital ICP® Signal Conditioner Model 485B39 manufactured by The Modal Shop; The accelerometer is manufactured by PCB Piezotronics, model 352A24.

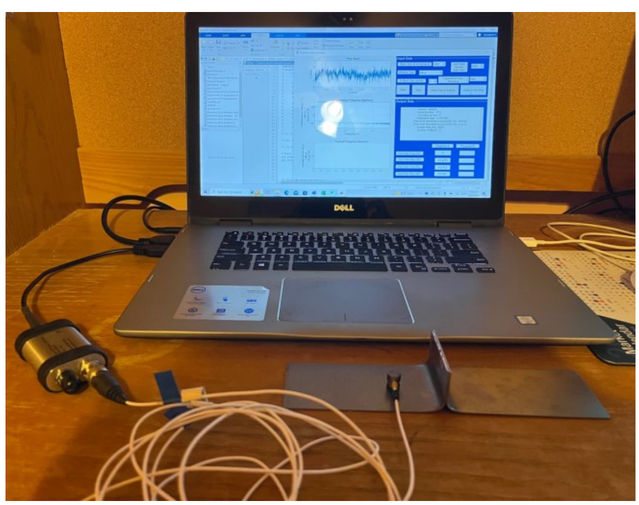

**Figure 14. Data Acquisition System**

## 3.5 Fast Fourier Transform Software (Data processing)

Modified MATLAB software: The FFT execution is accomplished by using a modified MATLAB code for signal processing. The original MATLAB code was part of a signal processing software (open source), it was modified to allow for amplitude data and FFT blocks to be exported for analysis. The modification of the existing MATLAB code includes:

1. Obtain peak value identification for amplitude associated with each frequency values per FFT block.
2. Forming a new dimension based on top 10 amplitude values and FFT blocks.
3. Export amplitude and FFT block values for posttest analysis.

## 3.6 Signal Sampling Theorem and Conversion Factors

In order to perform FFT the data transfer parameters need to be set up to conform to the Fourier analysis format. This includes: the data block size defined as Discrete Fourier Transform. It ranges from $64 = 2^6$ to $32{,}768=2^{15}$, and currently set as 2048 ($=2^{10}$) meaning each block will contain 2048 bits of discrete data points; The sampling frequency $S_f$ is defined as how fast the software reads (retrieves) the discrete points of data within a block. It is currently set to be 8000 Hz in the range of (8000, 11025, 16000, 22050, 32000, 44100, 48000) Hz. The overlap size, defined as overlapping portion of the data block to the next block of data, is currently set as 25%. This will smooth the ends of each block data to have a continuous curve for the output spectrum plot. The conversion factor is determined by the relationship of the block size, sampling frequency and external force frequency. The tables of conversion factors under each scenario are shown in Table 4.

**Table 4. FFT Block and Loading Cycle Conversion Table**

| | | | | |
|---|---|---|---|---|
| Applied loading Frequency(Hz) | 6 | | | |
| FFT block size (N) 2^11 | 2048 | 2048 | 2048 | 2048 |
| Data sampling rate $S_f$(Hz) | 8000 | 11025 | 16000 | 22050 |
| Td=N/$S_f$ | 0.256 | 0.18576 | 0.128 | 0.09288 |
| Loading frequency(Hz) | 6 | 6 | 6 | 6 |
| FFT block to cycles | 1.536 | 1.114558 | 0.768 | 0.557279 |
| | | | | |
| FFT block size (N) 2^12 | 4096 | 4096 | 4096 | 4096 |
| Data sampling rate $S_f$(Hz) | 8000 | 11025 | 16000 | 22050 |
| Td=N/$S_f$ | 0.512 | 0.371519 | 0.256 | 0.18576 |
| Loading frequency(Hz) | 6 | 6 | 6 | 6 |
| FFT block to cycles | 3.072 | 2.229116 | 1.536 | 1.114558 |
| | | | | |
| FFT block size (N) 2^13 | 8192 | 8192 | 8192 | 8192 |
| Data sampling rate $S_f$(Hz) | 8000 | 11025 | 16000 | 22050 |
| Td=N/$S_f$ | 1.024 | 0.743039 | 0.512 | 0.371519 |
| Loading frequency(Hz) | 6 | 6 | 6 | 6 |
| FFT block to cycles | 6.144 | 4.458231 | 3.072 | 2.229116 |

Description of Table 4: The applied loading frequency (Hz) is the setting by the manufacturer for analyzing the joint assembly with designated frequency, in current study, it is 6 Hz. The size of the FFT block is set as 2048, sampling rate is set at 8000 Hz, thus the conversion factor between the FFT block and the machine running cycle is 1.536. As the size of the block increases, the conversion factor increases, which means the output resolution is becoming coarse. One the other hand, if the sampling rate is higher, for example 11025, the conversion rate is 1.114558 which means the resolution is higher than 1.536 which is the current value. It was found that when keeping the conversion factor between 1~2 the results are satisfactory.

## 3.7 Data Processing in Amplitude-FFT Block Space

During the continued data processing from time domain to frequency domain, the output of the frequency-amplitude plot can be observed as another input data for amplitude value study. The reason: monitoring and analyzing the frequency change due to a loaded sample's internal damage is difficult as described 2.4. When they system has a high noise level, multiple frequency values were generated by the non-linearity and tracking of these values is not productive in terms of identifying the crack initiation and different types of damage. This study observed that if the top 10 amplitude values associated with each frequency values generated by the system could be tracked and analyzed in a new dimension formed by Amplitude and FFT Blocks, there is a good correlation between the movement of the Amplitude-FFT Block space and the actual damage of the sample. This observation was also based on the results of video analysis during the sample's destructive test. (See Section 4.9).

## 3.8 Numerical data processing procedures

The below steps were developed to process the data from FFT (MATLAB) and obtain the new data plot for further analysis for the impact of the sample damage:

1. Obtain peak (top 10) values of amplitude associated with each frequency per FFT block.
2. Obtain the maximum value of each 10 values per FFT block. See Figure 15.
3. In the array formed by the FFT block and the amplitude values (from 2 above), split the amplitude value column into maximum and minimum values columns. See Figure 16.

4. Plot the maximum and minimum values (y-axis data) in the FFT block domain (x-axis). See Figure 17.
5. If the plot needs more resolution, repeat process 3 and 4 until the desired resolution is obtained.

2. Obtain max values from each FFT block

1. Obtain Data from FFT

| FFT Block | Val 1 | Val 2 | Val 3 | Val 4 | Val 5 | Val 6 | Val 7 | Val 8 | Val 9 | Val 10 | Abs Max |
|---|---|---|---|---|---|---|---|---|---|---|---|
| 1 | 59.00317 | 20.80558 | 22.03185 | 21.24217 | 168.2695 | 4012.104 | 523.6459 | 298.8053 | 26.56397 | 10.7957 | 4012.104 |
| 2 | 35.46054 | 13.47103 | 161.5442 | 374.0038 | 2593.576 | 528.2546 | 62.03865 | 262.1503 | 22.146 | 11.31172 | 2593.576 |
| 3 | 15.4887 | 15.14178 | 157.5192 | 53.84916 | 959.6013 | 409.8329 | 45.20857 | 207.2894 | 168.9082 | 12.84742 | 959.6013 |
| 4 | 14.9806 | 175.2532 | 1740.457 | 434.7967 | 151.2872 | 150.9823 | 26.10676 | 10.33104 | 12.28585 | 10.96004 | 1740.457 |
| 5 | 18.41358 | 188.3792 | 2699.359 | 393.6248 | 196.9921 | 194.7715 | 39.74747 | 9.584631 | 9.819012 | 10.15033 | 2699.359 |
| 6 | 26.45017 | 192.5267 | 1122.62 | 446.0141 | 192.4516 | 189.8174 | 34.3618 | 16.06828 | 9.456487 | 16.77989 | 1122.62 |
| 7 | 38.52902 | 32.53606 | 24.237 | 169.2443 | 2769.702 | 336.0054 | 256.4262 | 25.06537 | 22.54503 | 25.71567 | 2769.702 |
| 8 | 19.12716 | 15.45468 | 176.2968 | 4146.549 | 437.9067 | 272.8777 | 24.49839 | 6.840899 | 14.47286 | 8.661266 | 4146.549 |
| 9 | 31.53355 | 35.6023 | 157.974 | 18.74178 | 3156.212 | 414.5461 | 200.0199 | 200.0844 | 17.86078 | 18.7192 | 3156.212 |
| 10 | 11.49036 | 186.2734 | 384.1298 | 1483.452 | 378.909 | 199.3728 | 170.5276 | 38.31086 | 4.939422 | 3.922225 | 1483.452 |
| 11 | 52.62009 | 129.9482 | 2916.245 | 355.9593 | 105.8437 | 117.1388 | 189.0877 | 35.79731 | 12.73912 | 13.58657 | 2916.245 |
| 12 | 31.66094 | 137.9434 | 138.9697 | 296.3236 | 1786.76 | 408.1031 | 225.4307 | 163.0634 | 24.16555 | 20.89324 | 1786.76 |
| 13 | 16.94045 | 17.24784 | 192.0922 | 24.80058 | 265.4721 | 296.7747 | 381.7836 | 379.7503 | 250.3531 | 13.98219 | 381.7836 |
| 14 | 41.55931 | 30.31633 | 27.25304 | 190.6545 | 1053.743 | 418.1466 | 303.4521 | 8.574896 | 6.50457 | 11.52847 | 1053.743 |
| 15 | 15.74842 | 14.30375 | 15.26296 | 182.8229 | 1777.984 | 470.1243 | 40.90847 | 166.8831 | 171.2932 | 26.8842 | 1777.984 |
| 16 | 89.3521 | 30.57195 | 183.0415 | 1737.688 | 334.523 | 128.7605 | 175.0261 | 12.09977 | 12.22729 | 7.991042 | 1737.688 |
| 17 | 21.92562 | 190.3129 | 2517.736 | 291.8569 | 211.7838 | 162.5194 | 9.44282 | 3.876342 | 16.20128 | 13.88376 | 2517.736 |
| 18 | 152.5868 | 4342.009 | 308.4866 | 55.68374 | 269.2249 | 32.76671 | 9.20381 | 8.653641 | 17.45641 | 4.695921 | 4342.009 |
| 19 | 33.681 | 179.2036 | 3841.25 | 326.7958 | 234.4755 | 316.7329 | 13.51731 | 14.85699 | 15.16073 | 10.93494 | 3841.25 |
| 20 | 143.5168 | 65.36209 | 1203.479 | 414.9576 | 294.9237 | 13.5358 | 12.79365 | 7.701359 | 14.08872 | 11.11497 | 1203.479 |
| 21 | 35.23459 | 31.79592 | 147.9593 | 25.26307 | 1600.431 | 512.6242 | 179.7759 | 174.5096 | 21.70594 | 18.63735 | 1600.431 |
| 22 | 38.70295 | 66.8501 | 76.38817 | 83.51327 | 206.5898 | 269.684 | 136.2058 | 2222.095 | 424.8465 | 230.4946 | 2222.095 |

3. Export new array for next step

**Figure 15. Numerical Procedure of Amplitude Data Analysis**

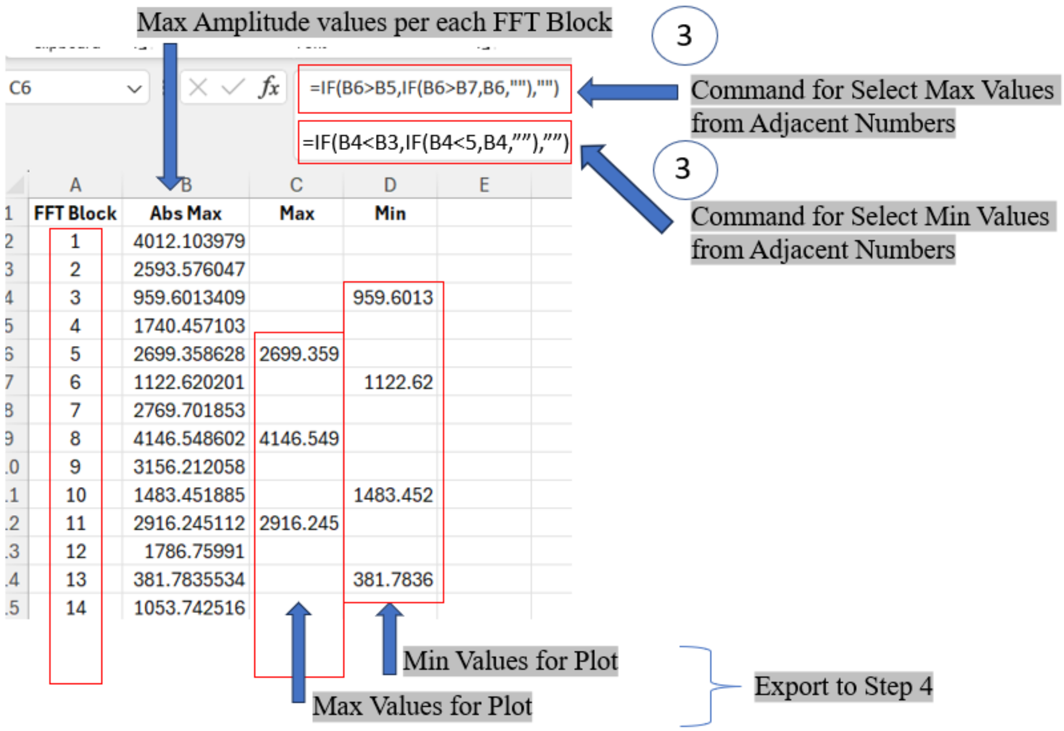


**Figure 16. Numerical Procedure for Amplitude Data Analysis (Continue)**

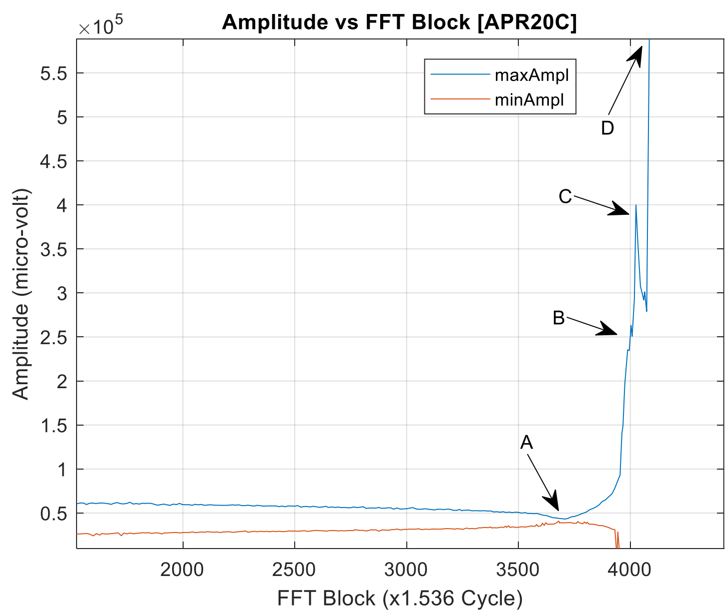


**Figure 17. A completed Amplitude-FFT Block Diagram after 2 iterations of eliminating middle values (noise)**

These steps will ensure the system noise is filtered out. The amplitude values from this process will be the maximum value per each FFT block and will capture the spike of movement of amplitude during the cyclic loading process.

### 3.9 Characteristics of the Amplitude-FFT Block Diagram (CP)

For CP samples, refer to Figure 16, a typical amplitude-FFT block diagram presents information about a sample's vibration status vs. FFT block (equivalent to timeline, or cycle line). The maximum value curve is positioned on top, and the minimum value curve is at the bottom. The end of the curves representing the failure point where the sample is completely separated is designated as "D". The horizontal axis represents the FFT Blocks which is equivalent to time and cycles. From the left end, the top and bottom curves are initially horizontal with a slightly convergence towards the point "A" where a "bottleneck" is formed. Once the curves pass point "A", they diverge and move away from each other. The top curve continues to move higher to point "B". With a little hesitation, the top curve moves higher to "C" and drops down to a higher-low point then increases to a much higher point "D". These characteristics were found in every coach peel sample diagram. The exact physical meaning of the points "A" to "D" are the focus for this study in Chapter 4. Although the shape and form are slightly different for each individual sample, they all have similar format which will be analyzed against the monotonic load-displacement diagram and the video analysis for further interpretation.

### 3.10 Characteristics of the Amplitude-FFT block Diagram (LS)

For LS samples, shown in Figure 17, the amplitude-FFT block diagram presents a different set of characteristics:

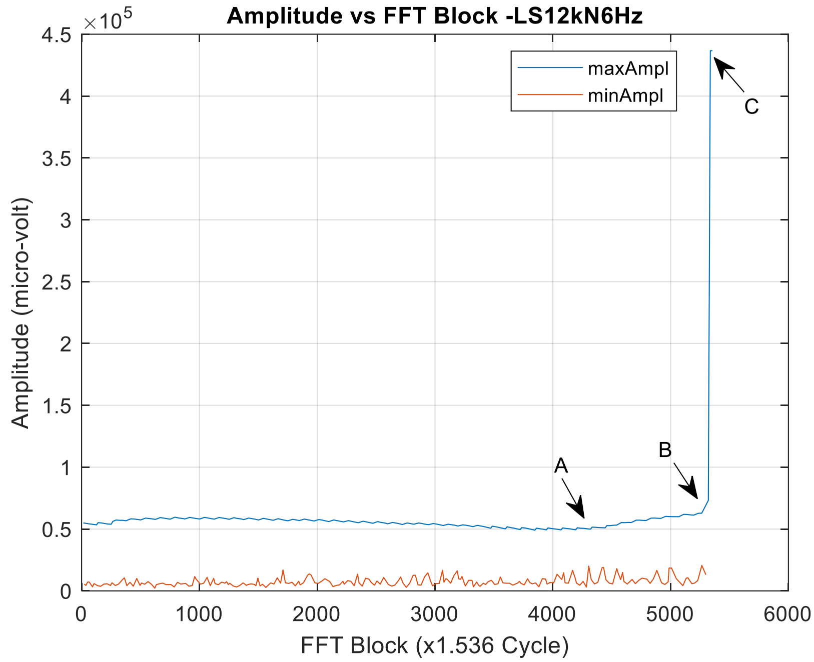


**Figure 18. Lap Shear sample amplitude FFT block diagram**

Beginning from the left, the top and bottom amplitude curves are initially constant versus FFT blocks, then the top curve decreases slightly representing the effect of strain hardening of the sample. The top line turns slightly downwards to form a "bottleneck" with the bottom curve at point "A". This can be explained as the adhesive material being plastically deformed so the amplitude value drops. After passing "A" the top curve moves higher to point "B" indicating the debonding occurred causing the slight rise in amplitude, see Figure 18. Right at the point "B", the top curve turns vertical to the high point "C" which represents the sudden failure of the sample (complete separation). All lap shear samples tested possess a similar format and the mechanical interpretations will be studied in Chapter 4 where comparison to the monotonic load-displacement diagram will be part of the tool to develop full understanding of this configuration.

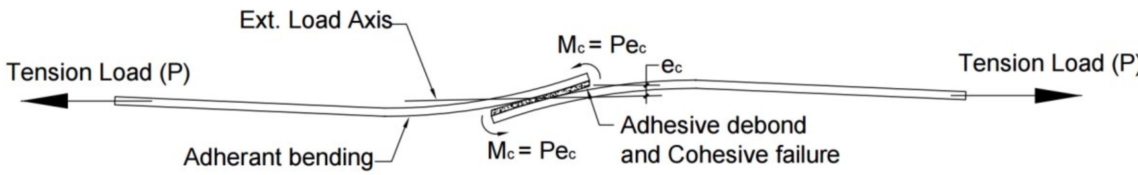


**Figure 19. Typical Lap Shear Sample Failure Mode**

## 3.11 Summary and Discussion

Fatigue testing involves a detailed planning process, design of testing samples, configuration of testing procedures, samples making and execution of the testing. Video recording and analysis is part of the process. In this study, the videos were taken by an iPhone-XSR. Microsoft Excel was used for post test data analysis. MATLAB was used for executing FFT and graph plotting. The reason that the top 10 amplitude values were selected to perform data analysis was to eliminate the noise in the output file after FFT, at the same time to retain enough spikes of amplitude values during the damage process. An arbitrary value of 10 was used to cover at least 6 fundamental mode shapes' movement in 3 directions (X, Y and Z). For most cases, only certain mode shapes could produce the most damage and matching loading direction, the combination of the result would generate maximum spikes, the set up for 10 values yielded good results for the samples tested.

CHAPTER FOUR

ANALYSIS OF TEST DATA AND RESULTS ANALYSIS

## 4.1 Analysis for CP samples

In order to fully understand the CP joint behavior, the monotonic load-displacement diagram was used to compare with cyclic loading cases. When placing the amplitude-FFT diagram and the load-displacement diagram side by side, (Figure 4 and Figure 17), a one-to-one mapping can be drawn to understand the progression of each phase of damage. The fatigue testing set up specified “load control” as the testing parameter. As shown in Figure 20 the effect of this set up is not a true constant load as increase of the moment arm occurs due to crack propagation.

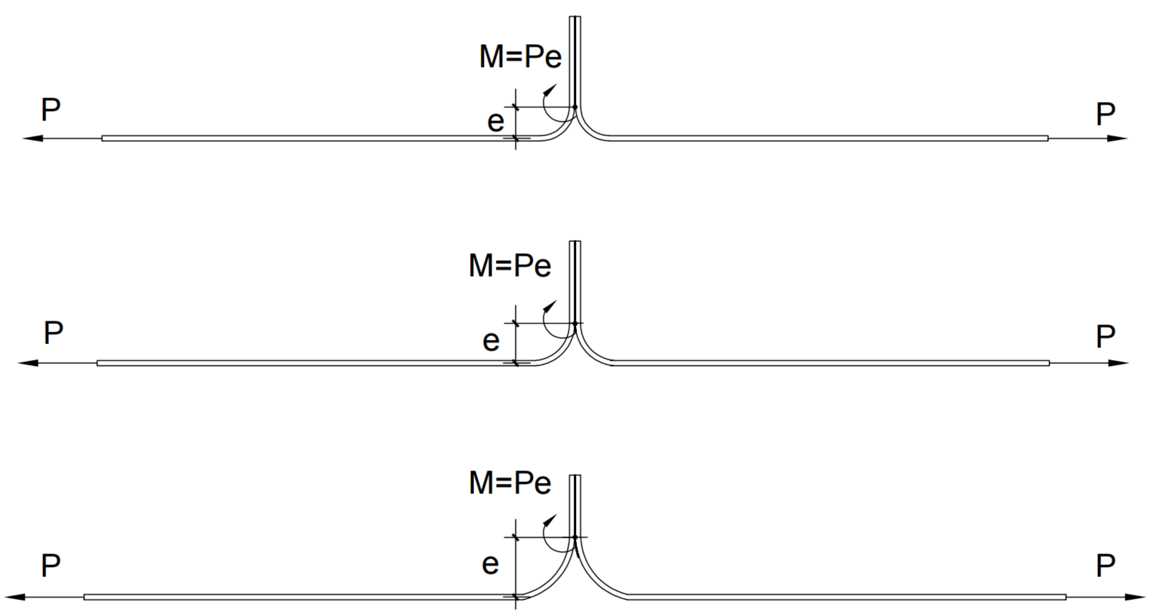


**Figure 20. Increased Moment Arm for CP Joint**

**Figure 21. Bent Sheets for the Final Stage of Pull Test**

## 4.2 Comparison of cyclic load and monotonic load for CP sample

A detailed list of comparison points between monotonic and cyclic loading is listed in Table 5.

**Table 5. CP joint failure points comparison between monotonic and cyclic load**

| **Coach Peel Sample Load-Failure Comparison** | | | |
|---|---|---|---|
| Monotonic Loading | | Cyclic Loading | |
| 0-A | Almost elastic curve, slightly strain softening | 0-A | Amplitude curve flat and slightly downward trend, coinside with strain softening curve |
| A-B | Adhesive failure, displacement increase, load drop | A-B | Debonding occurred, crack initiated, amplitude climb |
| B-C | Cohesive failure started, reaction force dropped with small increase in displacement | B-C | Crack propagation, adhesive material separation, amplitude increase on a fast pace |
| C-D | Cohesive failure quickly spread to entire bonded area, displacement increase, sample completely failed (separation) | C-D | Internal damage area increased, amplitude shoot up to new high |

Correlation between the monotonic loading and cyclic loading (CP) was found to be:

0-A: As loading increases, the adhesive layer starts experiencing stretching, with resulting strain softening, see Figure 4.

A-B: At point A, the tension stress becomes larger than the adhesive strength and crack initiation occurs. For the monotonic loading case, the overall strength becomes less due to reduced area of adhesive in the sample. For the cyclic loading case, the amplitude starts increasing due to loss of stiffness, as a result, a ramp up of amplitude can be seen on the graph (Figure 16). This action continues till the end where adhesive resistance becomes zero, the stress from the load is transferred to cohesive resistance, as can be seen there is a small delay at point B.

B-C: For the monotonic load case, the full load is resisted by cohesive strength at this point. As the load increases, the displacement does not increase due to weaker cohesive strength compared to the adhesive strength and the load value drops. In the amplitude graph, as cohesive strength takes over, the cyclic load results in less cohesive resistance due to loss in area, stiffness drops and amplitude increases. Since the cyclic loading is force controlled, as more cycles occur, there is less area remaining thus stiffness decreases. The amplitude increases up to point C.

C-D: In the monotonic graph (Figure 4) as cohesive resistance becomes diminished, the displacement increases, and load starts to level off. At the same time, the steel sheet bending capacity starts to increase as part of the remaining resistance. For the amplitude graph (Figure 16), as the amplitude graph increases to point C, as less cohesive resistance remains due to stiffness loss, the system starts relying on the bending capacity of the steel sheet where the decrease after point C can be an indication of such resistance which resists the increase in vibration amplitude. As the steel sheets' bending capacity continues to resist external force, the amplitude curve drops to the minimum value after point C. At this point, the two sheets are separated due to the bending resistance being completely exhausted, and the vibration amplitude drastically increases following an almost vertical line, as free vibration occurs. Figure 20 shows the bending sheets condition, the curvature of bending becomes more rounded after a certain height where cohesive strength declines and can no longer resist the pulling force.

### 4.3 Load test data analysis for LS samples

For Lap Shear samples, a one-on-one mapping of each failure point is related to Figure 5 (monotonic load-displacement diagram) and Figure 17 (cyclic amplitude-FFT block diagram). The failure of the LS samples can be described as a polarized action at the adhesive area, one end failed by adhesive failure and the other end failed by cohesive failure as shown in Figure 22.

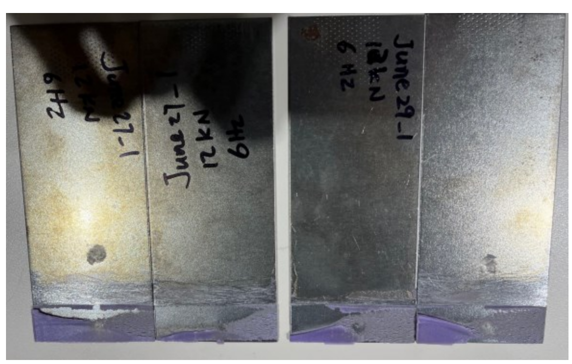


**Figure 22. Failure mode for typical LS sample**

Figure 23 shows the progression deformation of LS samples under increased loading. As the load increases, the eccentricity between the loading center line and the adhesive edge increases, this moment of P*e combined with shear stress will continue increase with the external load (P-constant) and increasing eccentricity "e" until the combined stress at each free end of the adhesive joint exceeds the adhesive bonding capacity (when "e" reaches "$e_c$"). The joint fails with the adhesive failure followed by cohesive failure. The total failure occurs in a very short time with a sudden separation of the metal sheets. As the result of plate end moment, there are sign of end (corner) deformation due to bending condition.

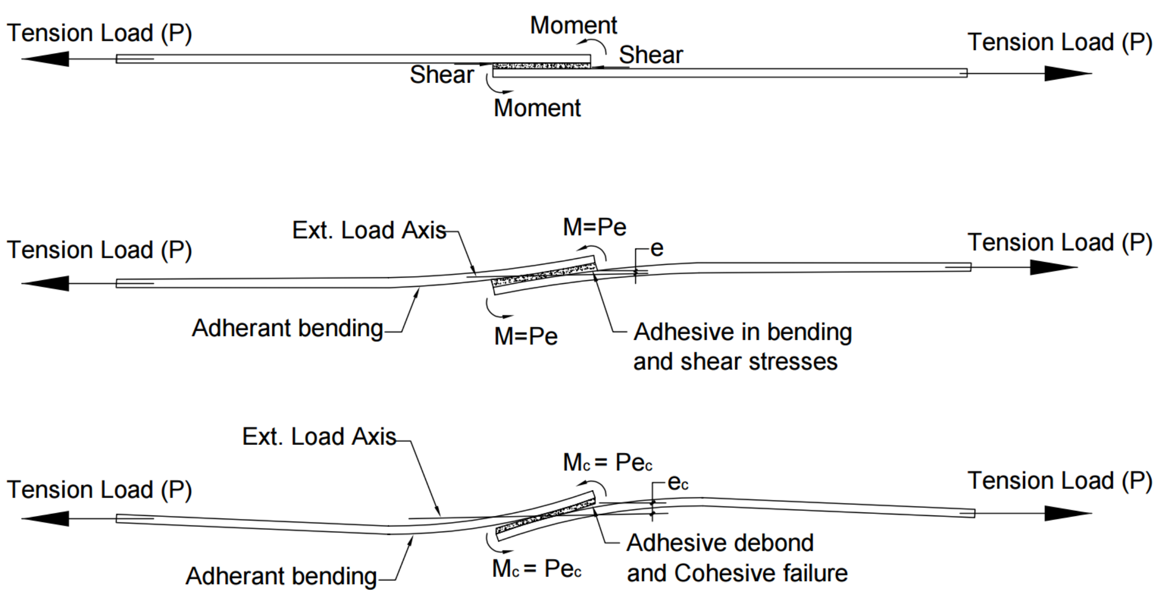


**Figure 23. LS Sample Debonding Progression Under Tension Load**

## 4.4 Comparison of cyclic load and monotonic load for LS Sample

A detailed list of comparison points of monotonic load versus cyclic load is listed in Table 6.

**Table 6. Comparison of failure point for LS sample**

| Lap Shear Sample Load-Failure Comparison | | | |
|---|---|---|---|
| Monotonic Loading | | Cyclic Loading | |
| 0-A | Almost elastic curve, slightly strain softening followed by strain hardening due to rising curve | 0-A | Amplitude curve flat and slightly downward trend, coinside with strain softening curve to the point A then slightly rise up indicates strain hardening phase |
| A-B | Adhesive damage accumulative phase for adhesive and cohesive failures | A-B | As damage in adhesive and cohesive accumulation, internal stiffness reduce and amplitude increase |
| B | Both adhesive and cohesive damage and propagation complete, remaining adhesive area drop to the breaking point the sample failed suddenly | B | Crack (adhesive and cohesive) propagation, increased damage area causing stiffness drop to the critical point. Amplitude value turns up |
| B-C | General failure occurred, no displacement, force drop, sample separated | B-C | Internal damage causing sample separation, free vibration occurred with amplitude shoot up |

Correlation between the monotonic loading and cyclic loading (LS):

Refer to Figure 18 (amplitude-FFT) and Figure 5 (Monotonic LS) for the following descriptions.

0-A: As loading increases, the adhesive layer starts experiencing increased shear stress.

A-B: At point A, the shear stress starts causing large deformation and adhesive debonding starts to increase. At this point more cyclic loading caused more area damage (adhesive) and at some point, between A-B, the cohesive damage started accumulating. For the cyclic loading case, the increase of damage causes stiffness to drop and amplitude to increase.

B: The accumulated area of damage (both adhesive and cohesive) increased to the critical point where the balance of internal resistance and external force was out of balance and the sample failed suddenly.

B-C: The sample failed with separation, no displacement and the force dropped. For the amplitude graph, the complete separation causes free vibration and the amplitude rapidly increased. One notable observation: the corner of the cohesive failure experienced some rotation of the sheet which indicates a large enough force to cause the sheet to bend. Lap shear failures are separated by an adhesive failure side (corner) and cohesive failure side (corner), they never occurred in the same side as shown in Figure 22.

### 4.5 Correlation to Displacement-Cycle Plot for CP sample

Based on the FFT block conversion factor to cycle count relation described in Chapter 3.6, the following detailed analysis demonstrates one real sample's cycle count for each damage (failure) mode. Refer to displacement-cycle diagram (Figure 24) and amplitude-FFT diagram (Figure 17).

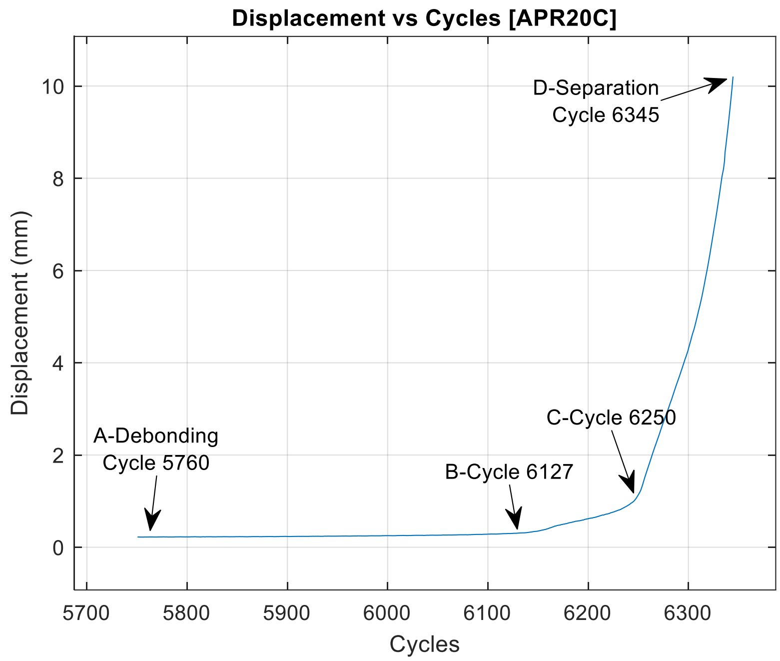


**Figure 24. Displacement-cycle diagram (MTS)**

Since the starting point of the FFT can be different than the MTS loading system, the way to match the block number of debonding to the machine cycle is to line up the failure point and count backwards. As shown in Figure 17 for a coach peel sample test, the sequence of events from 0 to A, B, C and D are marked with executed FFT blocks. The end point of the FFT block is 4087 at point D. The crack initiation point A is at block 3706. Table 3 shows the comparison of each stage sequentially corresponding to each point between Figure 23 and Figure 18. It can be seen that the amplitude curve divergent point (the change in slope from negative to positive) is at point A. Point B indicated crack propagation and initiation of cohesive failure, this event was accompanied with the slope change to a steeper angle. From this point till C the amplitude curve increased steeply with a few FFT blocks indicating an accelerated internal damage. From point C to D the sample experienced further crack propagation with cohesive failure, adhesive separation, amplitude (and displacement) increased at a higher rate with reduction of adhesive attachment for each added loading cycle until total sample separation.

Calculation of cycles and FFT blocks:

D-C=4087-4025=62 blocks x 1.536 = 95 cycles

C-B=4025-3945=80 blocks x 1.536 = 123 cycles

B-A=3945-3706=239 blocks x 1.536 = 367 cycles

Total cycles between debonding and total separation: 585 cycles

The number of cycles when debonding occurred was 5760 (point A). The calculated points at B and C are accurately located where the slope of the displacement curve changed indicating a different internal damage type. From A to B, crack initiation (adhesive failure) occurred, and propagation progressed. From B to C, cohesive failure began, and propagation progressed until total sample separation at point D.

After placing all the cycle count points (from A to D) above into Figure 24, each of the points representing a turning point in the displacement-cycle diagram, meaning that the slope at each point changed due to a different failure mode.

### 4.6 Correlation to Reaction Force-Cycle Plot for CP sample

Obtaining MTS gripper force data is part of the post data analysis process. This information can be helpful to confirm the type of damage throughout the sample testing process. See Figure 25.

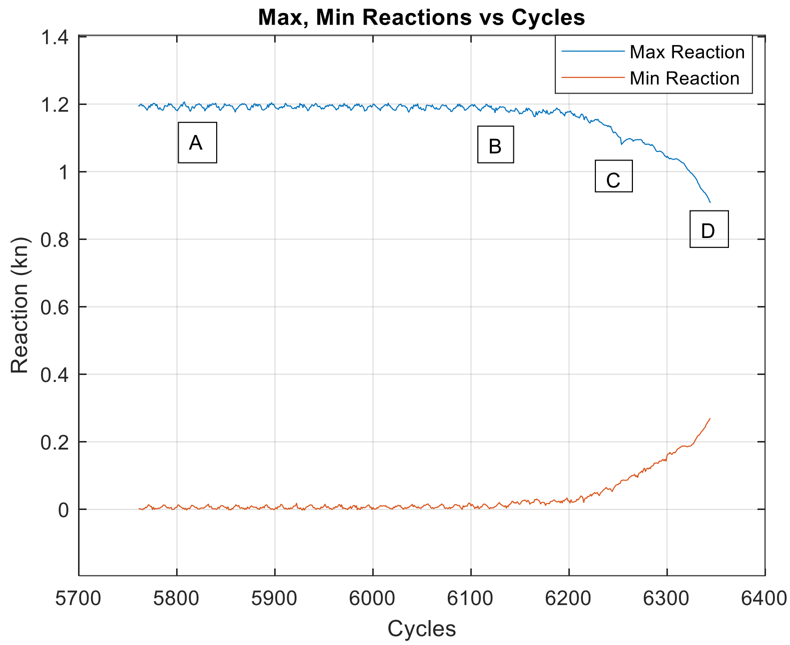


**Figure 25. MTS reaction force vs cycle count (CP)**

The MTS sensor for reaction on the sample is plotted with separation of maximum and minimum reaction values. The critical points A, B, C and D are mapped out according to the cycle counts based on Figure 25.

A-B: A near flat line or gradual descending line indicates the force on the sample was decreasing after debonding (adhesive failure started).

B-C: In this area cohesive failure initiated and propagated with a steeper slope at point C.

C-D: The sample lost most of the adhesive resistance due to cohesive failure, the steel sheets bending capacity decreased and the increased internal damage caused the reaction force to drop significantly. At point D, the sample was completely separated. This reaction diagram fits the concept for an object with an internal damage, the reaction force from MTS sensor applied to it becomes less as the stiffness reduces and the displacement increases.

### 4.7 Correlation to Displacement-Cycle Plot for LS Sample

Refer to Figure 26 and Figure 18 for the following descriptions related to cycle count:

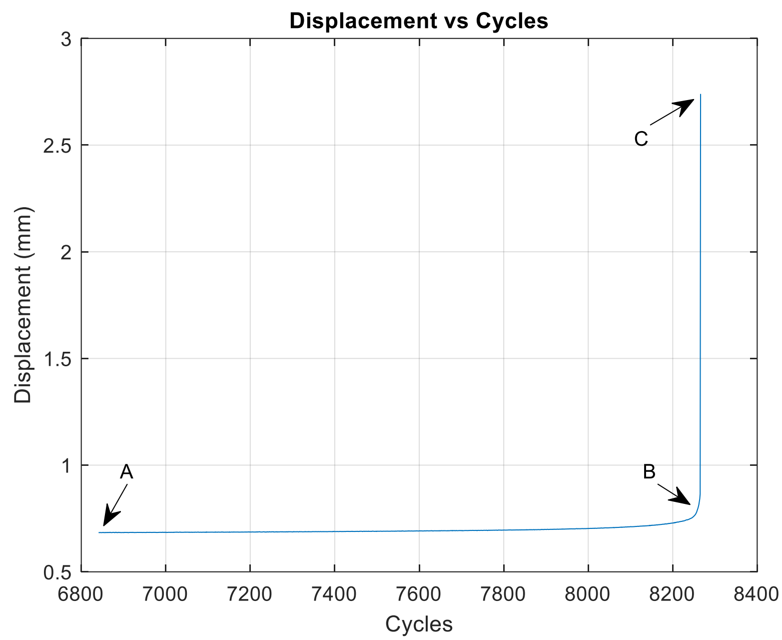


**Figure 26. Lap shear sample displacement-cycle plot**

Failure block: 5337 at 8266 cycle per MTS data, points B and C

Debonding block: 4305 at point A

Difference: 1032 x 1.536 =1585 cycles between debonding and failure

Debonding cycle: 8266-1585=6681

At point A of Figure 23, the debonding cycle is at 6681 which is the point where crack initiation with debonding and a combination of adhesive and cohesive failure began. The slope of A-B is slightly positive during the damage accumulation phase.

### 4.8 Correlation to Reaction Force-Cycle Plot for LS Sample

Figure 27 shows the sample reaction force (at griper) vs. cycle count curve. From point A to B the force is constant. Near point B the force dropped vertically indicating that sudden failure is the typical failure mode for a lap shear sample.

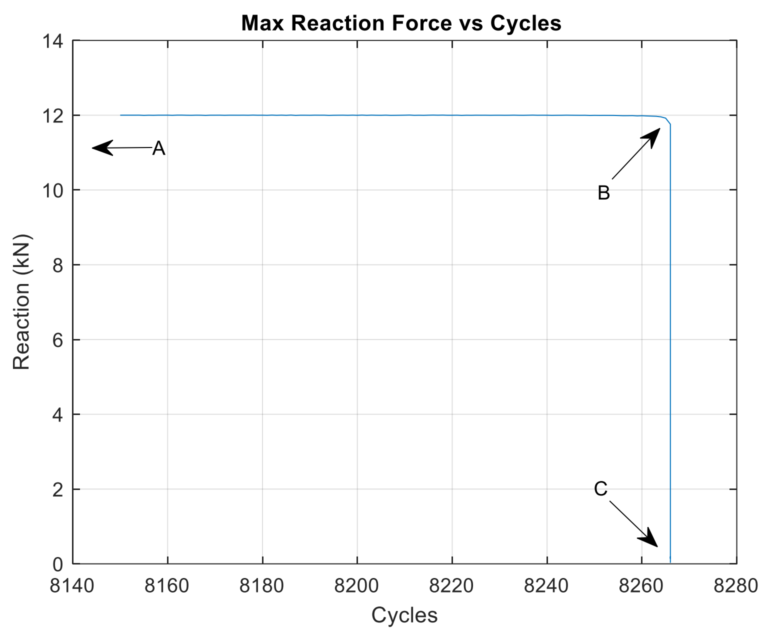


**Figure 27. MTS reaction force vs. cycle plot (LS)**

### 4.9 Video analysis of sample destructive test and collaboration on data plot

Study of video captured during destructive test for CP samples is part of the process to identify and confirm the debonding and other failure modes. A detailed frame by frame analysis for the sample's video is presented here with Table 7 showing each critical stage with time scale and corresponding cycle. Figure 24-27 show the captured image at each failure stage with time scale indicated.

**Table 7. Video collaboration with experimental observation**

| MTS-Amplitude-Video Coordination Example | | | | | |
|---|---|---|---|---|---|
| Specimen: | APR26 | Max Load: | 0.6 Kn | Mean Load: | 0.3 Kn |
| Amplitude data | Block A Debonding | Block B Adhesive Failure | Block C Cohesive Failure | Block D Separation | |
| FFT Block | 1948 | 2545 | 2771 | 2865 | |
| MTS Segment | 6396 | 8231 | 8925 | 9214 | |
| MTS Run Time(S) | 533.9000 | 686.6450 | 762.5330 | 768.6858 | |
| Backward Time(S) | 152.7550 | 75.9080 | 6.1328 | 0.0000 | |
| Video Time Scale | 1:36 | 4:08 | 5:24.9 | 5:31 | |

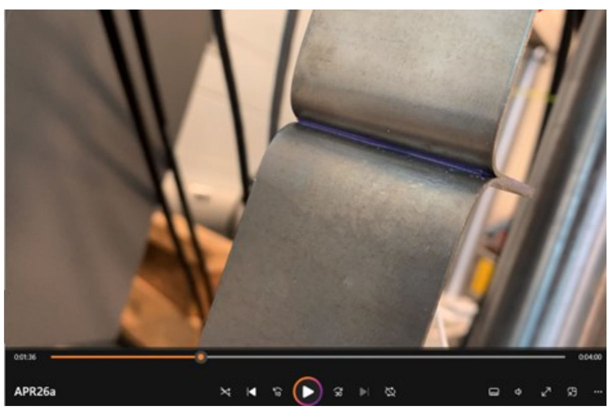


**Figure 28. Sample CP stage 0-A (time mark 1:36)**

Figure 28 shows the debonding block A and corresponding time in Table 7.

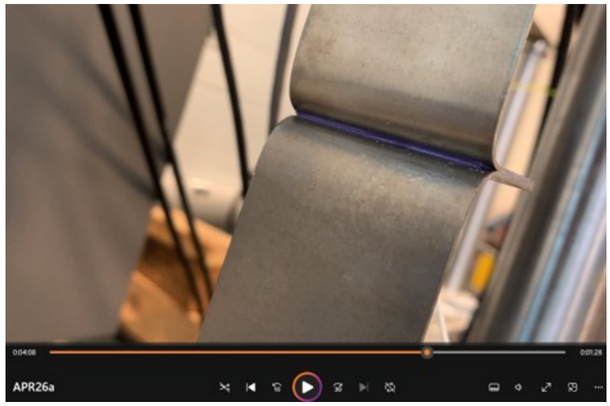


**Figure 29. Sample CP stage A-B (time mark 4:08)**

Figure 29 shows the adhesive failure at block B and time.

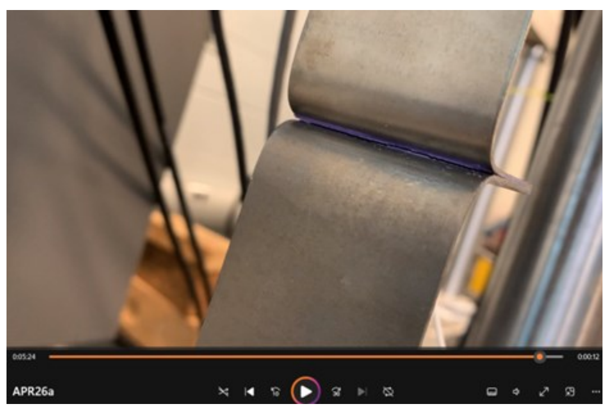


**Figure 30. Sample CP stage B-C (time mark 5:24)**

Figure 30 shows the sample cohesive failure at block C and time.

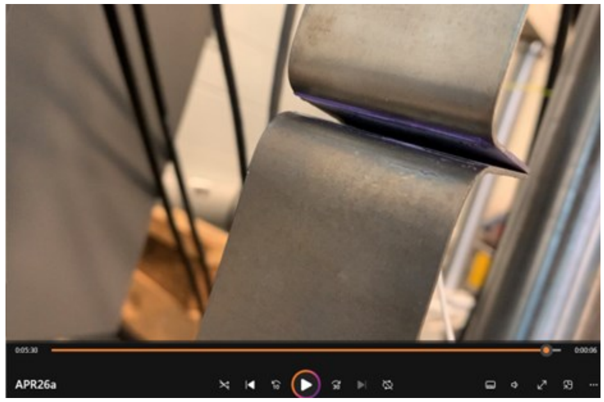


**Figure 31. Sample CP stage B-C (time mark 5:30)**

Figure 31 shows the sample separation at block D and time.

Due to the sudden failure of lap shear samples, the damage occurred so quickly that frame by frame video does not result in any clear damage stages.

## 4.10 Repeatability of current method

The current method is based on the intrinsic relationship between stiffness reduction (internal damage) and vibration amplitude (move higher when debonding occurred). There are external factors that can impact the quality of the test results (amplitude-FFT block diagrams). These factors are:

1. Geometric differences of one sample to the next one, the bend curve and radius of coach peel samples at stem. The symmetry of the two pieces and how they bonded together before the baking process.
2. Application of the adhesive, the thickness and uniformity of the adhesive layer can be a big unknown, especially at the corners, the consistency of thickness, there are no two pieces are made equal.

3. Assembly overall alignment: either coach peel or lap shear samples will need to be made as perfect as possible when joining.

With all quality measurements of above being satisfactory, the amplitude-FFT block diagrams shall all be looked consistent within each loading case. However, the diagrams obtained so far with more than 90 pieces tested, there are a lot of variations from one graph to another. This can be attributed to the quality of consistency problem. One way to resolve the problem is to calculate the standard deviation based on the variables (in terms of cycles to failure at each loading case).

### 4.11 Statistical data analysis for CP and LS results

Figure 32 shows the Boxchart for CP samples where more than 50% of samples cycle counts fall in between the 1st and 2nd quartile with no outliers for all the samples tested with 7 loading cases.

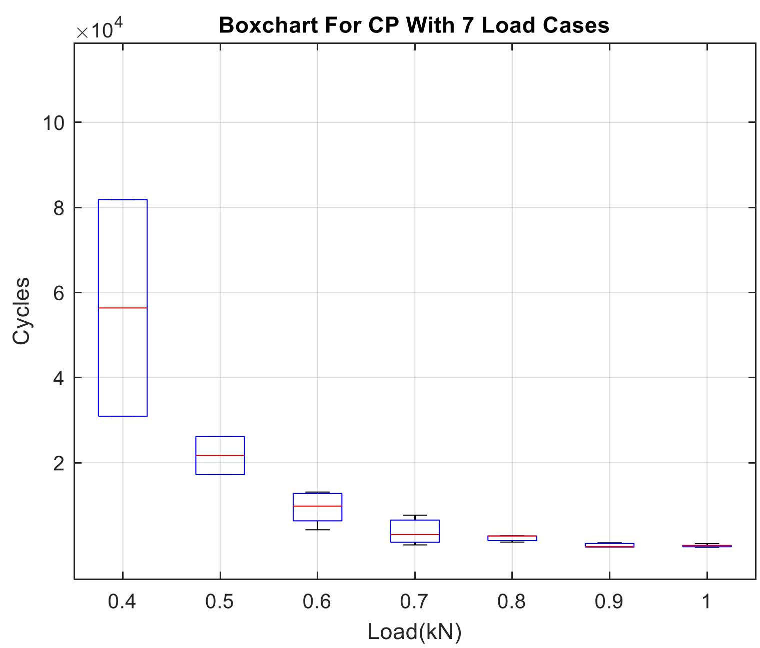


**Figure 32. Boxchart for CP samples cycle range with loading cases**

Figure 33 shows the Boxchart for LS samples with loading cases from 8kN~18kN.

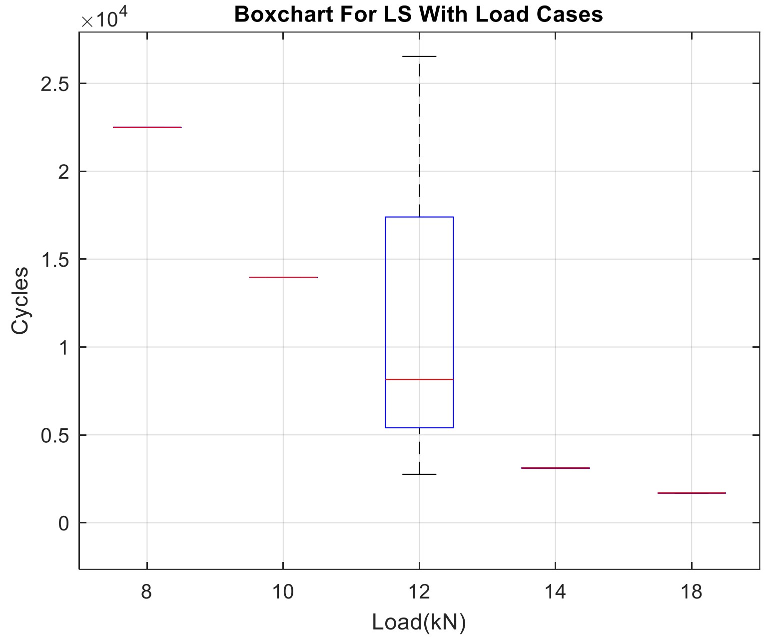


**Figure 33. Boxchart for LS samples with loading cases 8kN~18kN**

## 4.12 Summary and Discussion

In this study, coach peel and lap shear samples were tested with valuable data collected. It was found that for CP samples, the higher the load, the more elongation the amplitude diagrams were. This may be attributed to the fact that amplitude is directly related to the amount of force applied, therefore some distortions of amplitude-FFT plot result. One the other hand, amplitude plots with higher loads showed more details at certain damage stages (point B, C) which make the diagram easier to read. For the low curve (bottom curve) in an amplitude-FFT plot, sometimes the result from 2 consecutive data processing won't produce clear result as expected. In such cases, more data processing may be needed, or a scale factor (5-10 depending on scale) can be applied to derive a visible configuration, as indicated as “bottleneck”.

# CHAPTER FIVE

# CONCLUSIONS

The results from this study validated the fundamental relationship among stiffness, natural frequencies and associated amplitudes of an adhesive bonded joint. More importantly, debonding can be detected as long as the specimen's loading conditions fit the LEFM (linear elastic fracture mechanics) domain. Some specific conclusions are:

1. It is possible to detect debonding using amplitudes monitoring mechanisms and detect at what number of cycles the debonding occurs based on post test data processing results.
2. Strong correlations can be drawn with coach peel samples, in the amplitude curve for each stage of damage that matches the same damage in monotonic load – displacement, displacement - cycles and reaction - cycle curves.
3. Coach peel samples non-linear elastic characteristic (with gradual reduction of stress-strain curve between 0 and A) can provide more assistance than lap shear samples in identifying each critical point on an amplitude curve due to the nature of tension peeling effect.
4. In general, natural frequencies decrease in an object due to loss of stiffness in the direction of applied force. In the transverse direction, the natural frequencies may increase due to the gaps in between the cracked blocks. Amplitudes increase due to internal stiffness loss. In most cases, the increase in the amplitude will overwhelm the decrease of amplitude in different mode shapes, thus it can be used

as an indicator for damage analysis. When the separated amplitude curves' slope changes sharply at each critical point, this can be a good indicator to identify the debonding or a new status of damage such as adhesive failure transitioning to cohesive failure.

5. FEA modeling can help in positioning the accelerometer for a complex shape object so that the maximum damage of a potential internal damage can be identified by lining up the external force, based on the amplitude value change in certain mode shape and direction of the load, thus to enhance the result of the test.
6. Further research is needed to understand the crack initiation of multi welded and bonded joints in practical complex structures.

**Future work**

This study identified a few items which will require further study and implementation:

1. Integration of data processing: the current work depends on FFT exporting data for a separate process in order to plot the amplitude-FFT diagram. It would be more efficient to integrate the post test data process into the FFT software.
2. Expand this application to general solid mechanics, such as welds, solid metal components and other non-adhesive materials.
3. It is anticipated that testing of a component (sub-assembly with adhesive) can be conducted with no modifications required. Depending on the complexity of the component, multi-sensor approach may be appropriate to evaluate and identify the critical location where the stiffness is weak.

4. Based on implementation of #1 above, a wide range database can be established based on certain material testing results, graph and/or picture of amplitude-FFT plots, thus, to make it possible for real time monitoring system to provide alarm with instant recognition of patterns (based on slope of curve matching), for critical components.
5. "Waterfall" and or the "Color map" technique from special software such as "SpectralPLUS©" can be a useful tool for validation of current method. Additionally, in FEA simulation, comparing the stiffness matrix from before and after the crack embedment may present an alternative way to identify the crack initiation.

APPENDIX A

ADDITIONAL CP AMPLITUDE-FFT PLOTS

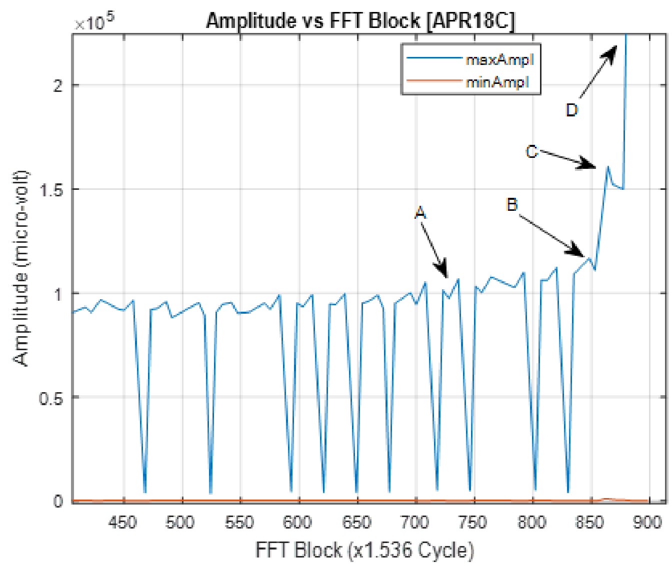


**Figure A1. Additional CP amplitude-FFT plot**

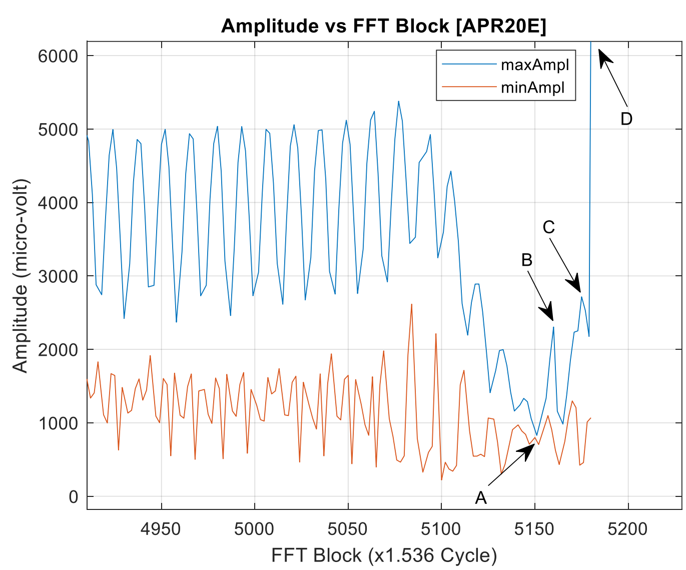


**Figure A2. Additional CP amplitude-FFT plot**

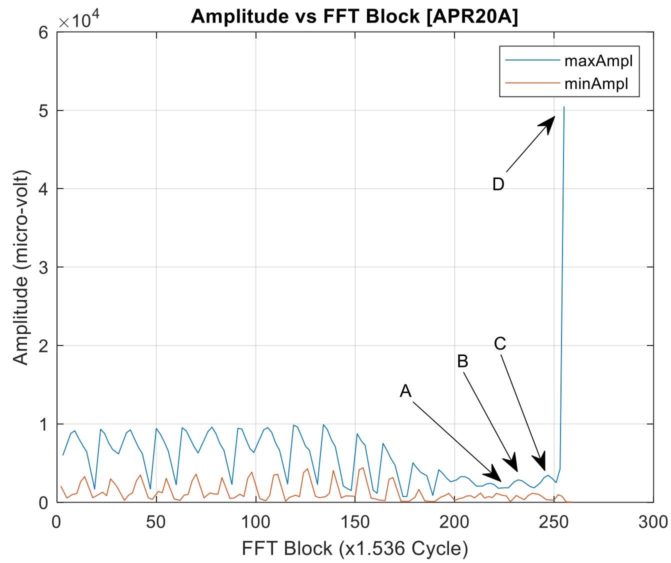


**Figure A3. Additional CP amplitude-FFT plot**

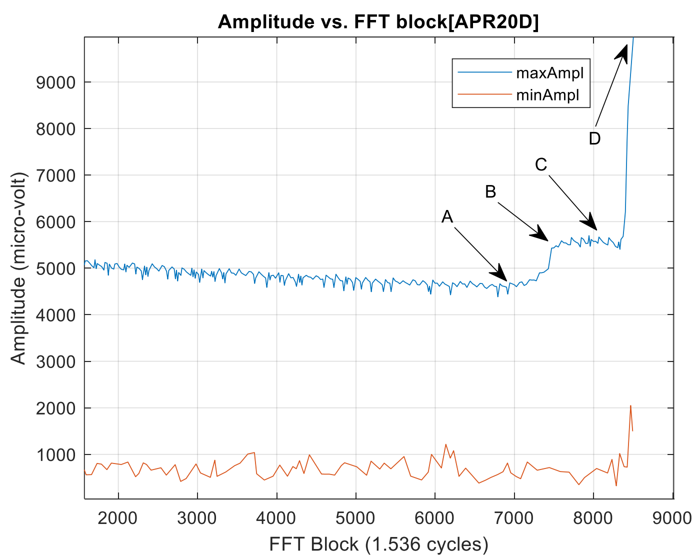


**Figure A4. Additional CP amplitude-FFT plot**

APENDIX B

ADDITIONAL LS AMPLITUDE-FFT PLOTS

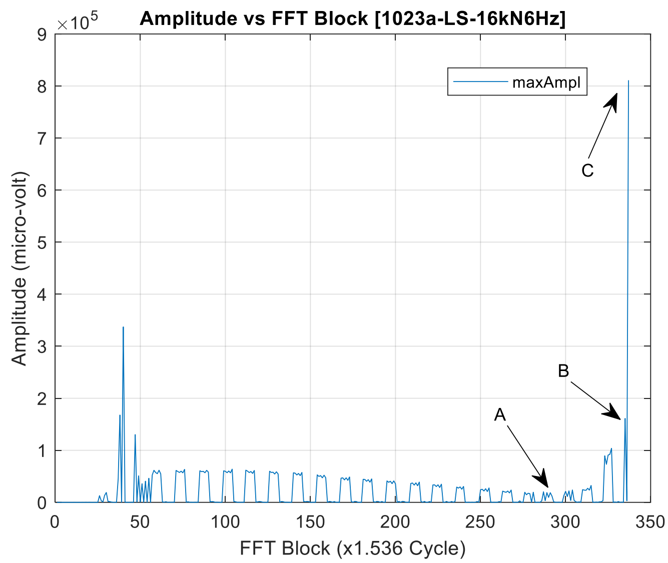


**Figure B1. Additional LS amplitude-FFT plot**

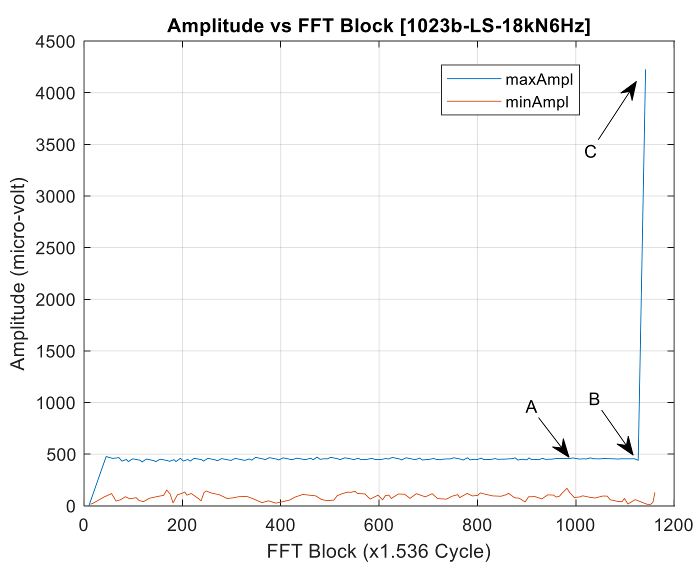


**Figure B2. Additional LS amplitude-FFT plot**

APENDIX C

PARTIAL SUMMARYOF SPECIMENS' LOAD AND FAILURE TABLE

**Table C1. Partial summary of specimens' load and failure progressions**

| Sample load table | | | | | | | |
|---|---|---|---|---|---|---|---|
| Figure | Sample # | Max load(Kn) | Mean load(Kn) | Block A | Block B | Block C | Block D |
| Fig 22 | APR18C | 1.6 | 0.8 | 728 | 848 | 864 | 890 |
| Fig 23 | APR20A | 1.2 | 0.6 | 222 | 232 | 247 | 255 |
| Fig 11 | APR20C | 1.2 | 0.6 | 3698 | 4003 | 4025 | 4087 |
| Fig 24 | APR20D | 1.2 | 0.6 | 6915 | 7525 | 8066 | 8521 |
| Fig 25 | APR26 | 0.6 | 0.3 | 1948 | 2545 | 2771 | 2865 |
| Fig 26 | APR20E | 1.2 | 0.6 | 5151 | 5160 | 5175 | 5183 |

# REFERENCES


1. M. M. Abdel Wahab, Fatigue in Adhesively Bonded Joints: A Review. Department of Mechanical Construction and Production, Ghent University, Technology park 903, 9052 Zwijnaarde, Belgium. October 2012.
2. Min Jung Lee, Tae Min Cho, Won Seock Kim, Byung Chai Lee, Jung Ju, Determination of cohesive parameters for a mixed-mode cohesive zone model. International Journal of Adhesion & Adhesives 30 (2010) 322–328, 2015.
3. Y.-M. Jen and C.-W. Ko, “Evaluation of fatigue life of adhesively bonded aluminum single-lap joints using interfacial parameters,” International Journal of Fatigue, vol. 32, no. 2, pp. 330–340, 2010.
4. Z. Z. Gao and Z. F. Yue, “Fatigue failure of polyethylene methacrylate in adhesive assembly under unsymmetrical bending,” Theoretical and Applied Fracture Mechanics, vol. 48, no. 1, pp. 89–96, 2007.
5. R. R. Gomatam and E. Sancaktar, “The effects of stress state, loading frequency and cyclic waveforms on the fatigue behavior of silver-filled electronically-conductive adhesive joints,” Journal of Adhesion Science and Technology, vol. 20, no. 1, pp. 53–68, 2006.
6. R. R. Gomatam and E. Sancaktar, “Effects of various adherend surface treatments on fatigue behavior of joints bonded with a silver-filled electronically conductive adhesive,” Journal of Adhesion Science and Technology, vol. 19, no. 8, pp. 659–678, 2005.

7. A. Graner Solana, A. D. Crocombe, and I. A. Ashcroft, “Fatigue life and back-face strain predictions in adhesively bonded joints,” International Journal of Adhesion and Adhesives, vol. 30, no. 1, pp. 36–42, 2010.

8. M. M. A. Wahab, I. A. Ashcroft, A. D. Crocombe et al., “Prediction of fatigue thresholds in adhesively bonded joints using damage mechanics and fracture mechanics,” Journal of Adhesion Science and Technology, vol. 15, no. 7, pp. 763–781, 2001.

9. M. M. Abdel Wahab, I. Hilmy, I. A. Ashcroft, and A. D. Crocombe, “Evaluation of fatigue damage in adhesive bonding: part 1: bulk adhesive,” Journal of Adhesion Science and Technology, vol. 24, no. 2, pp. 305–324, 2010.

10. M. Quaresimin and M. Ricotta, “Fatigue behavior and damage evolution of single lap bonded joints in composite material,” Composites Science and Technology, vol. 66, no. 2, pp. 176–187, 2006.

11. Z. H. Zhang, J. K. Shang, and F. V. Lawrence, “A back-face strain technique for detecting fatigue-crack initiation in adhesive joints,” The Journal of Adhesion, vol. 49, no. 1-2, pp. 23–36, 1995.

12. A. D. Crocombe, C. Y. Ong, C. M. Chan, M. M. A. Wahab, and I. A. Ashcroft, “Investigating fatigue damage evolution in adhesively bonded structures using back-face strain measurement,” The Journal of Adhesion, vol. 78, no. 9, pp. 745–776, 2002.

13. A. Bernasconi, L.M. Martulli, M. Carboni “Fatigue crack growth analysis in composite bonded joints by back face distributed strain sensing and comparison with X-ray microtomography” Department of Mechanical Engineering, Politecnico di Milano, Via La Masa 1, Milano 20156, Italy

14. Kaushar H. Barad, D. S. Sharma, Vishal Vyasb “Crack detection in cantilever beam by frequency-based method” Mechanical Engineering Department, Institute of Technology, Nirma University, Ahmedabad-382481, India

15. Rizos, P. F., Asparagathos, N. and Dimarogonas, A. D., 1990. Identification of crack location and magnitude in a cantilever beam from the vibration modes. Journal of Sounds and Vibrations. 138(3), 381-388.

16. Samir Khatir a, Kevin Dekemele a, Mia Loccufier a, Tawfiq Khatir b, Magd Abdel Wahab, Crack identification method in beam like structures using changes in experimentally measured frequencies and Particle Swarm Optimization.

17. A. Graner Solana, A.D. Crocombe, and I.A. Ashcroft
: Fatigue life and back face strain predictions in adhesively bonded joints. Faculty of Engineering and Physical Sciences (J5), University of Surrey, Guildford, Surrey GU2 7XH, UK.

18. Takahiko Sawada, Takashi Kawamori, Masahiro Matsunaga, Yosuke Fujiyasu, An experimental study for identifying crack initiation forces in single-lap bonded joints. Mechanical Engineering, Research & Development Group, Hitachi, Ltd., 832-2 Horiguchi, Hitachinaka 312- 0034, Japan b Research & Innovation Promotion Headquarters, Advanced Technology Research & Development Center, Hitachi Chemical Co. Ltd., 48 Wadai, Tsukuba-shi, Ibaraki 300-4247, Japan.

19. P. L. Rosendahl, Y. Staudt, C. Odenbreit, J. Schneider, and W. Becker, "Measuring mode I fracture properties of thick-layered structural silicone sealants," International Journal of Adhesion and Adhesives, vol. 91, pp. 64-71, 2019/06/01 2019, Doi: 10.1016/j.ijadhadh.2019.02.012.

20. Mihai LA, Goriely A. 2017, How to characterize a nonlinear elastic material? A review on nonlinear constitutive parameters in isotropic finite elasticity. Proc. R. Soc. A 473: 20170607. http://dx.doi.org/10.1098/rspa.2017.0607School of Mathematics, Cardiff University, Senghennyd Road, Cardiff, CF24 4AG, UK; Mathematical Institute, University of Oxford, Woodstock Road, Oxford, OX2 6GG, UK

21. Hencky H. 1928 Über die Form des Elastizitätsgesetzes bei ideal elastischen Stoffen. Z. Tech. Phys. 9, 215–220.